

Acoustic Navigation for the Autonomous Underwater Vehicle REMUS

by

Thomas F. Fulton

B.Sc., Ocean Engineering

United States Naval Academy, Annapolis Maryland (1992)

Submitted to the Department of Ocean Engineering
in partial fulfillment of the requirements for the degree of

Master of Science in Ocean Engineering

at the

MASSACHUSETTS INSTITUTE OF TECHNOLOGY

June 2000

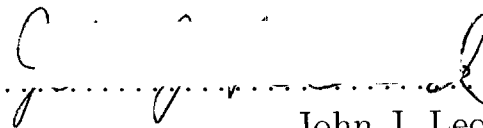
© Massachusetts Institute of Technology 2000. All rights reserved.

Author

Department of Ocean Engineering

May 5, 2000

Certified by.....



John J. Leonard

Assistant Professor of Ocean Engineering

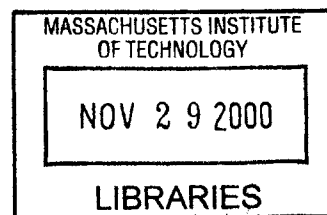
Thesis Supervisor

Accepted by.....

Professor Nicholas Patrikalakis

Kawasaki Professor of Engineering

Chairman, Departmental Committee on Graduate Students



ENG

Acoustic Navigation for the Autonomous Underwater Vehicle REMUS

by

Thomas F. Fulton

Submitted to the Department of Ocean Engineering
on May 5, 2000, in partial fulfillment of the
requirements for the degree of
Master of Science in Ocean Engineering

Abstract

The requirement for autonomous operation of Underwater Vehicles has led to several methods of navigation. One of the primary methods for navigation is Long Base-Line (LBL), where prepositioned acoustic transponders are used for a vehicle to find its own position. Due to vagaries of the acoustic path and difficulty in recognizing the direct path signal arrival, relying solely on acoustic transponder data results in navigation errors. These errors preclude an AUV from obtaining navigation accuracy better than a few meters over an operating area of several kilometers. By implementing an Extended Kalman Filter (EKF), vehicle state information is incorporated to the navigation solution, yielding an improved navigation fix over acoustic data alone. The future work in this area is in autonomous decision making for navigation. By taking out the 'man-in-the-loop', true autonomous operation is achieved, and the benefits of AUVs will be realized. This thesis examines the performance of our EKF, which uses the state data of heading and speed to improve acoustic fixes. The performance is illustrated by two methods. First, navigation data from missions at LEO-15, off the coast of New Jersey in July 1999, are post-processed using an EKF. Second, in-water experiments were conducted in Buzzards Bay, Woods Hole MA in April 2000, utilizing an on-line EKF. The results demonstrate the potential for smoother trajectory estimation, however reveal the potential sensitivity to EKF divergence when navigating in an array with only two transponders. This method is then evaluated as a springboard to autonomous decision making by the AUV.

Thesis Supervisor: John J. Leonard
Title: Assistant Professor of Ocean Engineering

Acknowledgments

This thesis is the culmination of two years of work with superb people at both Massachusetts Institute of Technology and Woods Hole Oceanographic Institution. I take this opportunity to gratefully acknowledge their guidance and assistance.

My utmost thanks to Professor John Leonard, who guided my efforts and kept me focused on the path to completion of this thesis. His constant enthusiasm and encouragement were an integral part of my studies. His guidance cannot be overstated, and I am very thankful for his leadership and vision.

Thank you to the WHOI Ocean Systems Lab, who make the REMUS vehicle an outstanding platform for both environmental assessment and research. The opportunity to work with a vehicle in an operational environment brought theories to life, and added the necessary reality to learned concepts. Chris Von Alt, Tom Austin, and Roger Stokey were always prepared to discuss ideas and implement them on the platform. Plus, they're a great bunch of guys.

My colleague during this work was Chris Cassidy, with whom I closely worked during this research. He has been a constant friend and valued sounding-board.

The members of the Design Lab were a source of support and friendship. Thank you to Rick Rikoski, Sung Joon Kim, Todd Jackson, Pubudu Wariyapola, and Rob Damus. Thank you to Fred Baker, Design Lab Manager, without whom I would have been adrift in a sea of technical computing minutiae.

Most importantly, thank you to the friends who have made my time in Boston so enjoyable. Rebecca Carrier, Tim Prestero, John Szatkowski, and Steve Terrio offered valued friendship and support. They reminded me it was important to keep life balanced in my pursuit of professional goals.

Finally, thank you to my family. Without the unwaivering support network of my parents and sister's families, I would not be where I am today. Thank you very much.

This thesis is supported by Office of Naval Research, via the National Defense Science and Engineering Graduate Fellowship.

Dedicated to my family - Thomas, Inge, Beate, and Helen - for their invaluable and continuous support, guidance, and love.

Contents

1	Introduction	9
1.1	Navigation requirement	9
1.2	Thesis road-map	11
2	A Review of Previous Research	13
2.1	Proprioceptive (on-vehicle) information	14
2.1.1	Dead Reckoning (DR)	14
2.1.2	Magnetic compass	15
2.1.3	Gyrocompass	16
2.1.4	Propeller shaft Revolutions per Minute (RPM)	17
2.1.5	Inertial Navigation System (INS)	18
2.1.6	Inertial Measurement Unit (IMU)	19
2.2	Environment Information	19
2.2.1	Acoustic methods	20
2.2.2	Global Positioning System (GPS)	22
2.2.3	Doppler Velocity Sonar (DVS)	23
2.3	Summary	23
3	LBL for REMUS operation	24
3.1	REMUS hardware description	24
3.2	REMUS navigation - SLOBNAV	26
3.3	Summary	29

4	Extended Kalman Filter for REMUS Navigation	30
4.1	Extended Kalman Filter description	30
4.2	Post-processed navigation missions - LEO-15, July 1999	36
4.2.1	Outliers	38
4.2.2	Gating	42
4.2.3	Divergence	43
4.2.4	Extended acoustic dropouts	45
4.2.5	Complete mission post-processing	49
4.3	Post-processing summary	51
4.4	On-line EKF missions - April 2000	54
4.5	Extended Kalman Filter navigation summary	59
5	Conclusions	63
5.1	Contributions	63
5.2	Future research	64

List of Figures

2-1	Range circles lead to two-beacon fix	21
3-1	REMUS Vehicle launch from small boat	25
3-2	Graphical User Interface for the REMUS vehicle	26
3-3	REMUS vehicles on bench	27
3-4	REMUS USBL hydrophone on vehicle nose	27
3-5	Dead reckoning transponder location for Sequential Long BaseLine Navigation (SLOBNAV)	28
4-1	Flow chart of Kalman Filter algorithm	31
4-2	Flow chart of Extended Kalman Filter algorithm	32
4-3	LEO-15 site as seen from the ocean bottom	36
4-4	LEO-15 buoy lines showing location of line N1-N6 and A1-A6	37
4-5	Vehicle trajectory for an 80 minute portion of July 19, 1999 REMUS LEO-15 mission	38
4-6	Range returns from buoys 5 and 6 for a 80 minute portion of mission LEO-15	40
4-7	Range returns for 7 minute portion of mission LEO-15	40
4-8	Vehicle track without gating LEO-15	41
4-9	Gating case. Vehicle track with gating, $\gamma=25$ LEO-15	43
4-10	Divergent case. Vehicle track with gating, $\gamma=14$ LEO-15	44
4-11	3σ position covariance LEO-15	45
4-12	Extended acoustic dropout effect LEO-15	46
4-13	Gated tracks for acoustic dropout portion LEO-15	47

4-14	Extended acoustic dropout gated ranges LEO-15	48
4-15	3σ position covariance for extended acoustic dropout LEO-15	48
4-16	Range returns for complete LEO-15 mission 7/19/99.	49
4-17	Gated tracks for complete mission LEO-15	50
4-18	Gated ranges for complete mission LEO-15	50
4-19	3σ position covariance for complete mission LEO-15	51
4-20	Summary of post-processing LEO-15	52
4-21	On-line EKF mission planned Buzzards Bay	53
4-22	On-line EKF mission completed Buzzards Bay	53
4-23	Buzzards Bay mission turn 1	54
4-24	Buzzards Bay mission turn 2	55
4-25	Buzzards Bay mission turn 3	55
4-26	Buzzards Bay mission turn 4	56
4-27	Close view of Buzzards Bay mission as planned	56
4-28	Close view of Buzzards Bay mission as completed	57
4-29	Buzzards Bay mission acoustic returns	57
4-30	Post-processed Buzzards Bay mission with gated ranges, $\gamma=1$	58
4-31	Post-processed Buzzards Bay mission with gated ranges, $\gamma=4$	58
4-32	Post-processed Buzzards Bay mission with gated ranges, $\gamma=25$	59
4-33	Summary post-processed Buzzards Bay mission with 3σ position co- variance	61
4-34	REMUS SLOBNAV fixes vs. EKF fixes	62
4-35	Position error plot of SLOBNAV fix vs. EKF fix	62

Chapter 1

Introduction

1.1 Navigation requirement

Accurate navigation is vital for effective Autonomous Underwater Vehicle (AUV) operations. It is defined as “the science of getting ships, aircraft, or spacecraft from place to place; *esp*: the method of determining position, course and distance traveled” [8]. Depending on the mission, navigation accuracy must range from the order of meters for long distance survey missions, to sub-centimeter accuracy for detailed bottom mapping for an archaeological site [33, 17].

Why is navigation important? It lies at the root of all AUV challenges today. The ability for a vehicle to concisely know its location, and to be able to return to that location, is vital. Mine survey, bottom mapping, or photographing geophysical phenomena require accurate navigation commensurate with the task. Detailed photomosaics of sunken vessels are possible with sub-centimeter navigation accuracy [34]. Operations in the water column with multiple vehicles require navigation accuracy on the order of 0.5 meters to map oceanographic phenomena such as a temperature or salinity front [25]. Docking with underwater nodes is required if the Autonomous Ocean Sampling Network (AOSN) concept is to be realized, which requires centimeter accuracy for the homing portion of the mission [9]. These scenarios only scratch the surface of the requirement for accurate navigation of AUVs, but are indicative of AUV missions that absolutely rely on robust, dependable navigation.

Navigation for vehicles such as ships, airplanes, and spacecraft has been studied for centuries. This depth of study has led to our mature understanding of the field, paving the way for the unparalleled navigation we enjoy today - worldwide shipping, air travel, lunar landings, and surgical military operations are made possible by precise navigation. AUVs, however, receive only partial benefit from the navigation advances of these fields. The distinct set of challenges faced by small vehicles operating in an underwater environment pose significant navigation hurdles. These challenges fall in two categories: 1) the limitations imposed by the ocean as a medium for communication and locomotion, and 2) size, weight, and power constraints for the navigation system.

The first challenge of operating in the ocean poses both communication and movement challenges. The ocean allows acoustic signals to propagate to great distances, but restricts the use of the electromagnetic spectrum. Further, currents tend to push the vehicle from its intended course, introducing errors to a dead-reckoned track. These two examples illustrate how the environment in which the AUV operates hinders accurate navigation.

The second challenge for the AUV lies in the physical size constraints and their effect on navigation. In general, decreased cost and power consumption yield decreased navigation accuracy. The size limitation of a vehicle drives the size, weight, and power boundaries for the navigation system. Since navigation requirements cannot be given unlimited size, weight, and power options, choices are made in system selection, which ultimately effect accuracy. This compromise between navigation requirements and available resources for the navigation system determines the navigation capability of the vehicle.

AUV navigation can be divided into two categories: 1) information derived from the vehicle itself (proprioceptive) and 2) information derived from the environment [8]. This dichotomy is based on the source from which the navigation information originates. The categories are shown below with further breakdown of the methods within each category.

1. Proprioceptive (on-vehicle) information

- dead reckoning (DR)
- magnetic compass
- gyrocompass
- propeller shaft revolutions per minute (RPM)
- inertial navigation system (INS)
 - inertial measurement unit (IMU)

2. Environment (off-vehicle) information

- acoustic methods
 - long baseline (LBL)
 - ultrashort baseline (USBL)
- global positioning system (GPS)
- Doppler velocity sonar (DVS)

These navigation subtopics are outlined and discussed in Chapter 2.

1.2 Thesis road-map

In this chapter, the history and importance of navigation were discussed. The challenging environment in which an AUV operates was surveyed, framing the problem which this thesis explores. Finally, the AUV navigation choices were divided between vehicle information (proprioceptive) sources and environment information sources, the starting point for further study. The structure of the rest of the thesis is as follows:

Chapter Two provides a summary of previous AUV navigation research and an overview of navigation methods. These methods are scrutinized with respect to accuracy, cost in both power and price, reliability, and autonomy, or how much human interface is required.

Chapter Three presents the details of Long BaseLine navigation for the REMUS vehicle. REMUS hardware is discussed, as well as the navigation algorithm created at Woods Hole Oceanographic Institution (WHOI) called Sequential Long BaseLine Navigation (SLOBNAV).

Chapter Four introduces the Extended Kalman Filter (EKF) proposed in this research. Outlier measurements, gating of outliers, divergence of the filter, and extended acoustic dropouts are discussed. The filter is analyzed both with post-processed navigation data from LEO-15 missions conducted in July 1999, and on-line EKF navigation in Buzzards Bay, MA obtained in April 2000.

Chapter Five concludes the dissertation with a summary of our research. Possible applications and improvements of the EKF implementation are discussed, and steps toward truly autonomous navigation decision making are presented. Finally, suggestions for future research in autonomous navigation are proposed.

Chapter 2

A Review of Previous Research

AUV navigation can be broken down to the following categories:

1. Proprioceptive (on-vehicle) information

- dead reckoning (DR)

- magnetic compass

- gyrocompass

- propeller shaft revolutions per minute (RPM)

- inertial navigation system (INS)

 - inertial measurement unit (IMU)

2. Environment (off-vehicle) information

- acoustic methods

 - long baseline (LBL)

 - ultrashort baseline (USBL)

- global positioning system (GPS)

- Doppler velocity sonar (DVS)

In this chapter, each of these methods will be examined and discussed.

2.1 Proprioceptive (on-vehicle) information

Proprioceptive information is obtained from the vehicle itself. It can be considered to be 'self-contained' on the vehicle, not needing external information from the environment. The two primary benefits of proprioceptive information are 1) it is an inexpensive mode of data collection, since the information is taken from within the vehicle, and 2) it is a non-detectable form of data collection. This inherent stealth is a result of not having to send out signals in the water to gain navigation information. Since it is passive data collection, it offers no signature of its operation to navigate. The various forms of proprioceptive information methods are described in detail below.

2.1.1 Dead Reckoning (DR)

The *dead reckoning (DR)* method is the oldest and simplest navigation method. DR consists of using the last known fix location, then advancing that fix to a current estimated position by applying a direction of travel (heading) at a given speed (or a displacement over a given time). This method is the simplest in that it only requires three inputs, all observed from within the vehicle: heading, distance traveled, and time (or heading and velocity). This method, as any proprioceptive method without external correction, is very susceptible to drift, however. If no external information is used to update the DR position, the position error grows unbounded with time [8, 19]. Until the next fix is obtained, there is no check on the accuracy of the dead-reckoned track, and no bound on the error growth.

Since dead reckoning is such a simple method using readily available data, it is the most widely used navigation method. Most often, however, it is utilized in conjunction with another navigation method to bound error growth. Typically it is coupled with a navigation method that senses the environment, as discussed later in this chapter.

The next sections examine methods to gain input for dead reckoning. Heading and velocity are found on the vehicle via the magnetic compass, the gyrocompass, or

propeller shaft revolutions per minute (rpm).

2.1.2 Magnetic compass

The magnetic compass is perhaps the oldest form of proprioceptive information. It utilizes the earth's natural magnetic fields to supply the vehicle with heading information.

Magnetic compass information is easily attained from a low-cost, low-power sensor. Using only 7-15mA of current and costing around \$700, the 1.6 ounce Precision Navigation, Inc. TCM2 compass is economical in energy consumption, cost, and weight [14]. Though the magnetic compass offers precise measurements, the accuracy is low due to properties of the earth's magnetic field. Precision means the ability to obtain a measurement to several decimal places repeatedly, while accuracy means obtaining a measurement that is equal to the true value. The compass precision is advertised as 0.1 degree, with 0.1 degree repeatability. This is a relatively high precision, as a magnetic compass is inherently sensitive to react to the earth's magnetic field.

Regarding accuracy, the magnetic compass has two main sources of error - variation and deviation. Not only does magnetic north vary from true north depending on operating area on the globe (variation), but there is also a difference in magnetic and true compass readings depending on the direction the vehicle is heading (deviation). Variation is a function the earths magnetic core being offset from the geographical North Pole. Deviation is a function of permanent and induced magnetic fields of the vehicle affecting the local magnetic field. This deviation changes with vehicle heading and varies with the instruments which are in use [19, 20]. In addition to these two main errors, there are small scale, unmapped changes in magnetic fields over small operating areas [15, 29]. These fine changes fluctuate both with vehicle motor distortions to the magnetic field, and environmental disturbances due to ferrous objects or solar events which effect the earth's magnetic field, and are not accounted for by variation and deviation.

Variation and deviation are accounted for by using a magnetic to true correction

corresponding to operating area (for variation), then adding a correction from a deviation table corresponding to heading (for deviation). These corrections make the magnetic compass accurate to only ± 2 degrees, depending on heading and accuracy of the deviation table. This is an unacceptably large error, as a 1 degree heading offset results in a 17.5 meter error after only 1 km of travel.

The vagaries of the earth's magnetic field and the vehicle interaction with it make the magnetic compass the weak link for a dead reckoning vehicle. Though an inexpensive sensor which requires low power and reads the ever-present magnetic field, the magnetic compass cannot be used without external information improving the dead reckoned track. A small offset in heading, left uncorrected, will result in unbounded growth of position error, unless resetting corrections are made from other sources.

2.1.3 Gyrocompass

The gyrocompass provides heading information via a spinning set of masses that maintain their position in space. Rather than relying on the constancy of the earth's magnetic field, a gyrocompass utilizes the physics of a rotating body's tendency to maintain position in space, or a gyroscopic effect [16]. Once set to true north, the gyrocompass will continue to mark true north, while the moving vessel rotates about the gyrocompass. This proven method requires heavy spinning masses, adequate power to maintain the masses rotation, and a long (several hours) of settling time when first started.

Another type of gyrocompass, the ring laser gyro (RLG), also provides a measure of heading. Rather than relying on the torques of spinning masses as the conventional gyrocompass does, the RLG operates on the relativistic properties of light. Change in heading is measured by the phase shift of light traveling in opposite directions in a fixed ring on the vehicle [18]. When the vehicle rotates about the ring axis, the distance the light travels in the direction of the motion decreases. Similarly, the distance light travels in the opposite direction of the motion increases. This change in phase is measured to produce a change in heading measured by light. Very accurate

and lighter than the conventional gyro, the RLG seems to be an ideal substitute for the conventional gyro. Though its cost has come down in the past several years, it is still too expensive for a low-cost AUV.

Both types of gyrocompasses provide very precise, accurate heading information. The gyrocompass will tend to drift over time, however, with high quality commercial grade units drift rates of several km/hr [6]. To decrease this drift rate, vehicle position must be updated with environmental information, such as the Doppler Velocity Sonar or an acoustic method to bound the position error growth.

The disadvantages of the gyrocompass are weight (for the conventional gyro), power requirements and cost. These factors make the gyrocompass a feasible choice only for the most expensive, heavy vehicles.

2.1.4 Propeller shaft Revolutions per Minute (RPM)

There are two methods to estimate speed of the vehicle from the vehicle itself: 1) water speed past the hull and 2) propeller rotational speed. The first method measures the velocity of the water passing the hull of the vehicle with a mechanical sensor on the vehicle. This method can accurately obtain the speed of the water within the vehicle's reference frame, provided the measurement device is mounted away from the vehicle's disturbed flow. This method does not yield a speed over ground, however, as both the vehicle and the water in which it operates may be moving. Therefore, unless the currents are exactly known around the vehicle, an absolute vehicle speed is unobtainable.

The second method of measuring speed on the vehicle is to count propeller rotations. Propellers are cast with a designated advance per revolution. For example, a propeller may advance forward 4 inches in one revolution. Knowing this advance characteristic for the design propeller, and adding a slip factor to account for drag and inefficiencies, the speed of the vehicle can be estimated by the RPM of the propeller shaft. This is a crude method that results in a vague speed over ground. Vehicle hydrodynamics, vehicle turns, and water currents effect the relation between absolute vehicle speed over ground and propeller speed.

The propeller RPM method requires no special attached equipment, as it's a reading provided by the shaft motor. It is therefore a 'free' measurement, requiring no additional power or weight. The water speed past the hull, conversely, requires an additional appendage on the vehicle to physically measure the flow velocity. This protrusion effects the hydrodynamics and efficiency of the vehicle, increasing vehicle drag and power consumption. Ultimately, straight dead reckoning will result in position errors with unbounded growth, a problem that is amplified by submitting unreliable, inaccurate velocity measurements. To bound the position error growth, the dead reckoning must be augmented with updates from environmental measurements.

2.1.5 Inertial Navigation System (INS)

The *Inertial Navigation System (INS)* method utilizes gyrocompasses and accelerometers to ascertain position. It is comprised of an Inertial Measurement Unit (IMU) and a Navigation Processor (NP) to yield vehicle position [6]. This method uses an initial position, then navigates from that position continuously using gyroscopic heading and acceleration in all three axes [16, 19]. The acceleration can be integrated once to obtain velocity in all three directions, then integrated again for position. This yields a very accurate track, subject to the quality of the instruments and duration of the navigation without external resetting of position. Accuracies of 0.4% to 2% of distance traveled are attainable with an INS, without external position updates. By incorporating Doppler Velocity Sonar, accuracies of up to .01% of distance traveled have been reported [23]. This method is used extensively for spacecraft and submarine missions, where external data, such as GPS, is unavailable.

This method shows the limitations imposed by the size, weight, and available power in the AUV. INS is accurate to less than 0.4% of distance traveled if top grade, very expensive units are used. This accuracy is paid for in cost, size, and power requirements to such an extent that an AUV may be unable afford to utilize INS. For example, a \$6700 Crossbow Attitude and Heading Reference Sensor (AHRS) unit weighing 1.1 pounds and drawing 1.5 watts provides a heading accuracy of 1 degree, or a 2% error over distance traveled. To obtain a 0.2 degree accuracy, or a 0.4% error

over distance traveled, the INS costs \$60,000, weighs 10 pounds, and draws 30 watts [24]. These cost, weight, and power requirements are impossible for a small AUV to meet.

Ballistic missile submarines and spacecraft use INS, navigating at depth or in space for weeks at a time with minimal error growth. These vehicle systems, however, do not have a very low cost, as a \$150,000 AUV does. These systems further do not have very limited power, nor space constraints to the level of a 80 pound AUV. As the cost, weight, and power draw of the INS decreases to be suitable for an AUV, the quality of the INS decreases, and drift rate increases.

2.1.6 Inertial Measurement Unit (IMU)

The Inertial Measurement Unit is the heart of the INS method of navigation. The IMU is comprised of a gyro and accelerometer to output heading and accelerations of the vehicle in all three axes. Via the Navigation Processor, the INS then utilizes the measurements gained by the IMU to ascertain position. The IMU sensors are typically accurate to 1 nm/hr without external correction from the environment [6].

2.2 Environment Information

Environment information is obtained from sources located off of the vehicle. It requires some method of sensing the environment, then using that information to ascertain or improve position. The primary benefit is the incorporation of ground truth for navigation - providing an absolute, fixed source of information. The primary disadvantages are 1) this method typically requires higher costs, more power, and additional logistics (pre-positioned transponders, for example), and 2) lack of stealth. By emitting energy to the environment to gather information, the vehicle is offering tracking information. The environment information methods are described in detail in the following sections.

2.2.1 Acoustic methods

Acoustic methods utilize sound traveling in the ocean. Seawater denies the use of the electromagnetic spectrum at the data rates and distances required by an AUV, so electromagnetic communication and navigation via Global Positioning System (GPS) are impossible. Acoustic signals, however, travel great distances in the ocean, and are very capably exploited by creatures residing in the ocean [2]. Acoustic signals are used by whales and dolphins to communicate, hunt, and learn about their environment. By learning from these animals, we utilize the ability of sound to travel through water in the acoustic methods of navigation. In this method, transponders are prepositioned in the ocean, and their known location allows the AUV to navigate.

Acoustic methods are broken down to two categories:

1. Long BaseLine Navigation (LBL), and
2. Ultrashort Baseline Navigation (USBL).

These methods are similar in that they both measure range to the transponders, which requires the vehicle to have an accurate travel time for the interrogation of the transponder and the transponder response. This travel time forms a sphere around the beacon, on which the vehicle lies [13, 22]. Further, the 'BaseLine' to which both of these methods refer is the line of transponders whose position is known. The principal difference between LBL and USBL is that in LBL, the vehicle measures only range to the transponders. Conversely, in USBL, the vehicle measures both range and bearing to the transponder.

- **LBL navigation**

For LBL navigation, the travel times from two or more beacons are used to create spheres on which the vehicle lies. The depth is then measured, turning these spheres into circles at a constant depth, on which the vehicle is located. By using two transponders, two range circles are created which intersect, narrowing the possible vehicle position to one of two intersection points. If a third beacon

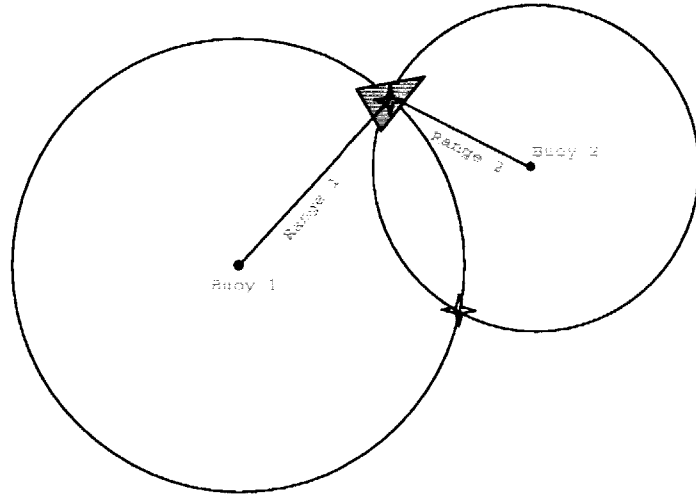


Figure 2-1: The travel times from the acoustic returns create range circles around each beacon. The intersection of these range circles provide the vehicle location.

is then added, or if the vehicle knows which side of the 'baseline' it's on, a fix can be obtained as the intersection point of the circles. The case of the two-beacon fix is shown in Figure 2-1. With a calibrated prepositioned transponder grid, accuracies of 1 to 2 meters are possible when acoustic propagation velocity is known [3].

The 'long' term in LBL refers to distance between the transponders, usually on the order of several kilometers.

- **USBL navigation**

For USBL navigation, the travel time of the signal creates a sphere on which the vehicle lies. This range is combined with a heading, or direction of acoustic return. By measuring depth, the vehicle can now obtain a fix from just one buoy, combining the bearing, range, and measured depth. Accuracy for USBL is expressed as a percent of range between acoustic source and receiver, and typical accuracy is about 1% to 2% of range [3].

The 'ultra-short' term in USBL refers to the distance between receiving hydrophone elements on the vehicle, which is on the order of centimeters. This small distance allows the vehicle to measure differences in phase of the arriving acoustic signal, hence angular measurement to the signal source.

2.2.2 Global Positioning System (GPS)

The *Global Positioning System (GPS)* method utilizes satellites circling the globe for precise position measurements. The system is based upon availability of multiple satellites passing within line of sight view from any point on the earth's surface. Each satellite transmits a unique signal, which includes precise time information along with its 3-dimensional position data [3]. A GPS receiver, after receiving signals from four or more satellites, can compute its 3-dimensional geodetic coordinates.

GPS on its own is accurate only to the order of several to tens of meters. This is due to ionospheric propagation and U.S. Defense Department introduced "selective availability" errors (to avoid delivering targeting-grade information to other nations). Most, if not all, of these errors can be removed with the use of Differential GPS (DGPS). A DGPS receiver collects both direct GPS satellite transmissions and signals from nearby fixed stations that provide error correction information, which are then used to greatly improve the accuracy of a position fix. Accuracies of less than a meter are attainable with the use of DGPS [3, 12].

GPS is very widely used for all applications where the electromagnetic signals can be detected, which is virtually all navigation requirements. These applications include air travel, sea shipping, and overland commerce. The only requirement for its use is the ability to detect the radio signals emitted from the GPS satellites. It is infeasible for AUV use, however, due to the attenuation of the electromagnetic signal through water. An AUV would have to surface to obtain a GPS fix, which is not desirable or possible in many missions that require great depth or covert operations.

The Florida Atlantic University Ocean Explorer AUV and Webb Technologies SLOCUM glider use dead reckoning, and surface intermittently to get a GPS fix to bound the error growth. Surfacing for a GPS fix is not possible for deep missions, where travel time from depth to the surface is prohibitive. Further, many mission profiles do not allow the AUV to surface, due to covert operations or vehicle traffic at the surface.

2.2.3 Doppler Velocity Sonar (DVS)

Doppler Velocity Sonar has been used with great success to obtain accurate measurements of speed over ground. In this method, several offset down-looking sonars are used to track the bottom of the ocean. By measuring the Doppler shift of the return of each beam, the speed of the vehicle over ground is obtained, both in the along-ship and across-ship directions. [33, 27].

DVS requires space and power on the vehicle, but not more than other sonars. By providing velocity measurements that are accurate to about 0.2%, the gains obtained in accurate earth-referenced velocity outweigh the space and energy considerations [6].

2.3 Summary

This chapter has reviewed previous research in navigation for vehicles. We have identified several methods of navigation that are used widely today. Our focus will be in LBL, due to the advantages of sound propagation in water, range, and the ground truth information of an environment measurement. We now proceed to discuss the REMUS system and LBL navigation for REMUS.

Chapter 3

LBL for REMUS operation

The previous chapter has reviewed previous research in navigation for vehicles and drawn us to look closely at LBL as a useful navigation method for AUVs. We begin this chapter by discussing the hardware for REMUS (Remote Environmental Measuring UnitS), then describing the LBL method created by WHOI called Sequential LOng Baseline NAVigation, or SLOBNAV.

3.1 REMUS hardware description

REMUS is a small, low cost AUV designed by the Ocean Systems Laboratory at Woods Hole Oceanographic Institution (WHOI OSL) [32]. A shallow-water vehicle rated to 150 meters, its primary mission is coastal survey and docking with seafloor observatories [1, 9]. In its basic configuration, the 135 cm (53 inch) long, 19 cm (7.5 inch diameter vehicle weighs 31 kg (68 pounds) in air, and is easily handled by a crew of two from a small boat as seen in Figure 3-1.

The standard REMUS survey configuration displacing 40 kg includes 1.2 MHz RD Instruments acoustic Doppler current profiler (ADCP), 600kHz Marine Sonics side scan sonar, conductivity, temperature, and depth recorder (CTD), and optical backscatter sensor (OBS). With the use of Lithium-ion batteries, the vehicle endurance is 15 hours at 3 knots, covering 80 km. The survey data collected is recorded on the onboard computer system which is based on the PC-104 architecture. Once



Figure 3-1: Vehicle launch from small boat. *Photo courtesy of WHOI OSL.*



Figure 3-2: Windows based Graphical User Interface for the REMUS vehicle. This program allows programming missions and downloading mission data when the vehicle is connected to a laptop or modem. *Photo courtesy of WHOI OSL.*

docked or connected to a computer on land, data is retrieved and the vehicle programmed via a graphical user interface which runs under Microsoft Windows. The REMUS interface is seen in Figure 3-2. Note the mission profile in the upper right corner of the screen, which allows the user to visually check the mission profile.

3.2 REMUS navigation - SLOBNAV

REMUS is equipped with an acoustic navigation systems that employs a dedicated PC-104 based DSP, enabling it to conduct long and ultra-short baseline navigation [28]. In addition, vehicles equipped with an ADCP are capable of bottom lock Doppler navigation. Often all three techniques are used within the same mission. The data from these sensor systems is combined in a position fixing technique that is currently implemented onboard the REMUS vehicle.

REMUS has both a transducer below the nose and hydrophone array on the nose of the vehicle for transmitting/receiving acoustic signals, as seen in Figure 3-3 and Figure 3-4. The vehicle transducer is used to transmit interrogation pulses to the pre-positioned transponder buoys. The transponder buoy reply is received by the transducer in the LBL configuration, and by the nose array hydrophone in the USBL configuration.

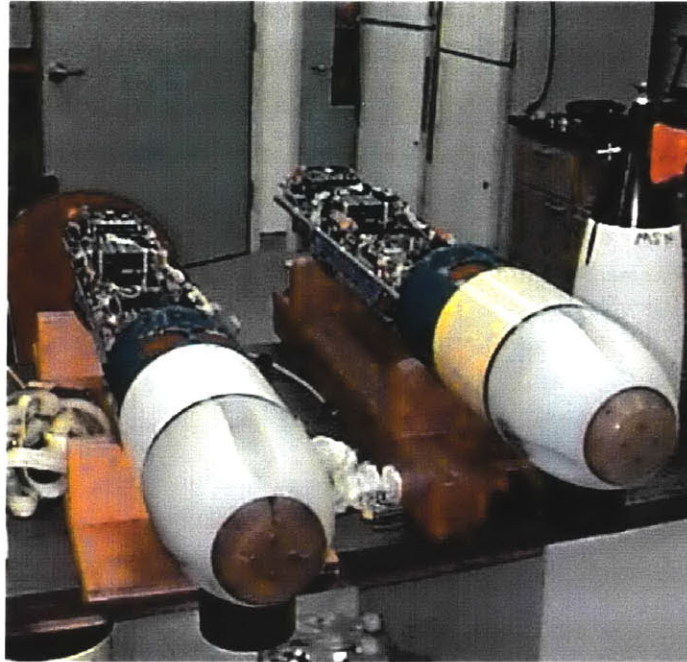


Figure 3-3: REMUS vehicles on bench. Note USBL hydrophone on vehicle nose, and LBL transducer under vehicle nose. Also visible are the four arrays for the ADCP, in the green section of the hull. *Photo courtesy of WHOI OSL.*



Figure 3-4: REMUS USBL hydrophone with 4 receive elements on vehicle nose, and LBL transducer under vehicle nose. *Photo courtesy of WHOI OSL.*

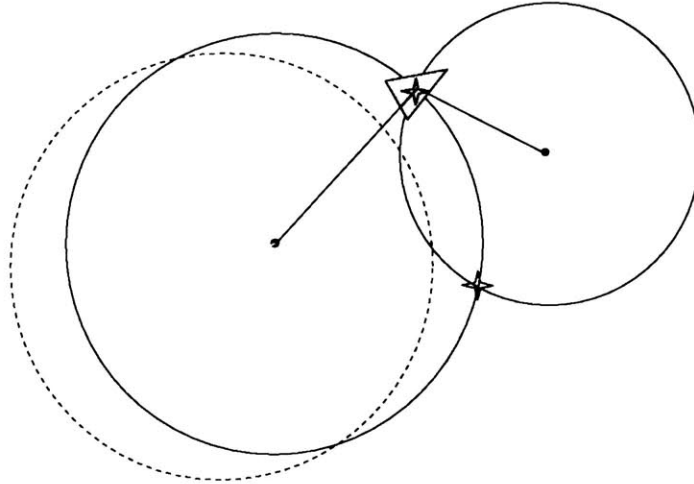


Figure 3-5: Sequential long baseline navigation entails moving a transponder location to a new dead reckoned position to obtain a fix with old acoustic data. In this figure, Buoy 1 is dead reckoned to an updated position to obtain a fix with acoustic information from Buoy 2.

For USBL, the nose array has four elements spaced at the four 'corners' of the nose, allowing the receipt time to vary at each element depending on the angle of the incoming signal front, as seen in Figure 3-4. This time delay, or angle of the wave front to the vehicle, gives an angle to the transponder as well as a travel time or range. This range and angle allows the vehicle to compute position from one signal return, making each interrogation cycle a complete navigation cycle.

The LBL cycle, conversely, requires that two separate transponders respond to interrogation cycles for a position fix. To save weight and limit power consumption, REMUS has only one tuned receiver board for incoming transponder signals. It interrogates one transponder at a time, and therefore only receives one range circle each interrogation cycle (see Figure 3-5). To obtain a fix, REMUS will dead reckon the last range circle from transponder A forward to the point where it receives a new range circle from transponder B. As seen in Figure 3-5, this 'sequential' interrogation and dead reckoning of old range information to the new range circle allows REMUS to obtain a fix without simultaneous receipt of transponder ranges, which is typical of an LBL net utilizing more than one receiver board on the vehicle.

Spurious ranges, and consequently spurious fixes, are a common problem for LBL navigation systems. Acoustic multipath, incorrect signal arrival time, and processing

errors lead to misidentifying the first arrival of an acoustic return. This fact requires a vehicle to reject spurious measurements or fixes.

REMUS handles the problem of spurious measurements in several ways [11]. At the start of each ping cycle, REMUS determines a range gate for the transponder it is interrogating. This determines the sampling window for the data acquisition cycle. Signals outside this minimum and maximum range aren't even acquired for processing. After acquisition, the signal must pass multiple signal to noise tests that enable REMUS to reject (for example) different transponders responding with different codes on the same frequency. Once these SNR tests are passed, the system attempts to compute a lat/lon fix based on the range information obtained. However, the result can be rejected if the new position is outside of an error circle surrounding the vehicles estimated position. This estimate grows linearly with time, and is set by the REMUS navigation programmer.

Using the REMUS onboard navigation algorithm, positioning accuracies of a few meters have been achieved in Navy sponsored tests. In November 1998, REMUS completed a star pattern around a target to study the ability of the sidescan sonar to relocate the target and navigate consistently about the target. The vehicle navigation accuracy was less than 3.5m in a challenging shallow water environment, where water depth was less than 10m [28].

3.3 Summary

In this section we summarized the REMUS hardware and navigation. We discussed the design mission, the sensors employed, and navigation methods utilized by REMUS. This discussion of the navigation will be continued in the next chapter, with the introduction of the Extended Kalman Filter.

Chapter 4

Extended Kalman Filter for REMUS Navigation

Having described Long BaseLine navigation, REMUS hardware and REMUS navigation (SLOBNAV), we now proceed to discuss the Extended Kalman Filter (EKF). We first consider the general EKF. Then, we examine post-processed REMUS mission data, describing outliers, gating, divergence, and extended acoustic dropout cases. Finally, we discuss the behavior of the on-line EKF.

4.1 Extended Kalman Filter description

The Extended Kalman Filter (EKF) is an optimal recursive data processing algorithm [5, 21]. Its primary benefit is that all new information, regardless of quality, is incorporated to estimate the vehicle state, and therefore position. This is accomplished by weighting the belief of each new measurement, and adding this information to update the state accordingly. The outline of the Kalman Filter (KF) and Extended Kalman Filter (EKF) are seen in Figure 4-1 and Figure 4-2. The reader is referred to Vaganay [31] and other references on Kalman filtering such as Bar-Shalom [5] and Maybeck [21] for more background on the EKF.

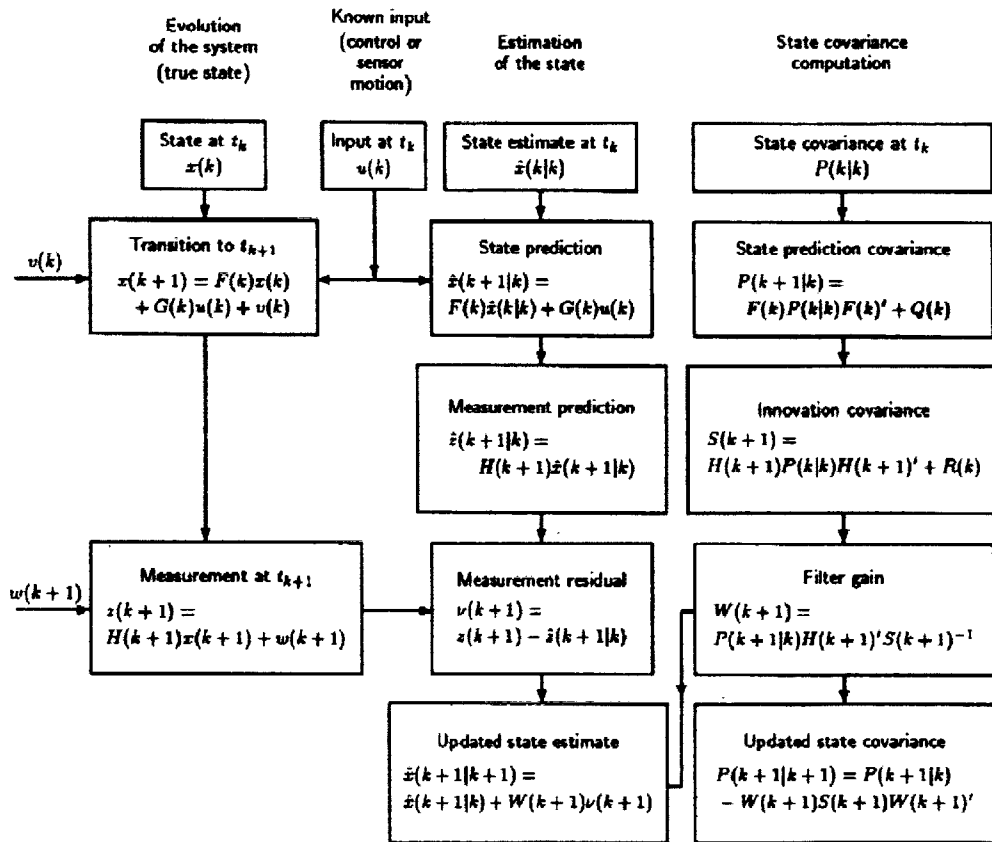


Figure 4-1: Flow chart of Kalman Filter algorithm. *Courtesy of Y.Bar Shalom [5]*

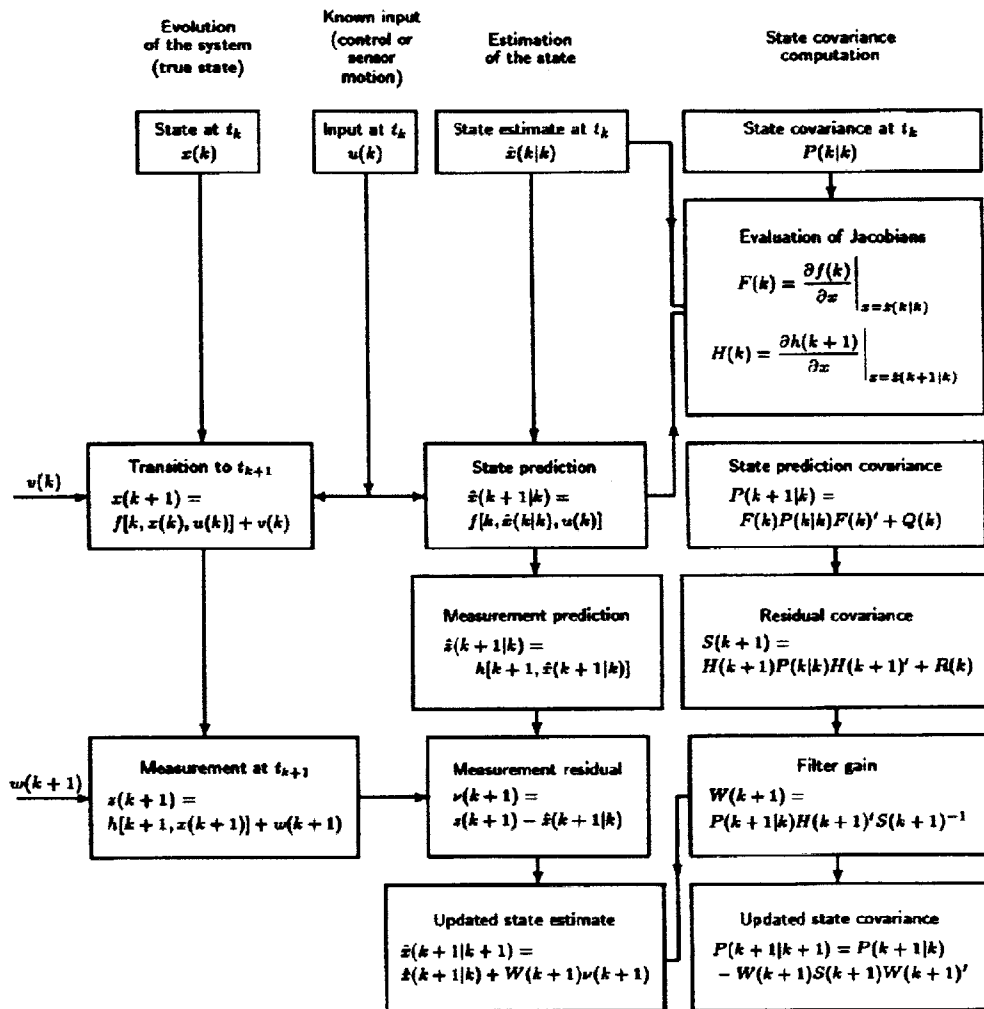


Figure 4-2: Flow chart of Extended Kalman Filter algorithm. *Courtesy of Y.Bar Shalom [5]*

The state vector, $\mathbf{x}(k)$, is

$$\mathbf{x}(k) = \begin{bmatrix} x \\ y \\ \theta \\ u \end{bmatrix} \quad (4.1)$$

Here, x and y denote position, θ is vehicle heading, and u is the vehicle velocity. The state transition function $\mathbf{f}()$ is given by

$$\mathbf{x}(k+1) = \begin{bmatrix} x(k+1) \\ y(k+1) \\ \theta(k+1) \\ u(k+1) \end{bmatrix} = \begin{bmatrix} x(k) + u(k) \cos(\theta(k))\delta(t) \\ y(k) + u(k) \sin(\theta(k))\delta(t) \\ \theta(k) + \Delta\theta(k) \\ u(k) + \Delta u(k) \end{bmatrix} \quad (4.2)$$

where $\Delta\theta(k)$ and $\Delta u(k)$ are known control inputs.

The plant model Jacobian $\mathbf{F}(k)$ is

$$\mathbf{F}(k) = \left. \frac{\partial \mathbf{f}(k)}{\partial \mathbf{x}} \right|_{\mathbf{x}=\hat{\mathbf{x}}(k|k)} = \begin{bmatrix} 1 & 0 & -u \sin(\theta)\delta(t) & \cos(\theta)\delta(t) \\ 0 & 1 & u \cos(\theta)\delta(t) & \sin(\theta)\delta(t) \\ 0 & 0 & 1 & 0 \\ 0 & 0 & 0 & 1 \end{bmatrix} \quad (4.3)$$

The measurement vector $\mathbf{z}(k)$ may vary in length depending on which information is available at each EKF cycle. Measurements of the vehicle heading, $\phi(k)$, are provided by a compass, and measurements of the vehicle's forward speed, $U(k)$ are provided by a Doppler velocity sonar. These quantities are updated at a rate of 1 Hz. Range measurements, however, are provided from the REMUS sequential long baseline mode system at a rate of approximately .2 to .5 Hz. The measurement vector, therefore, varies in length for each update of the filter, depending on which measurements are available when the EKF is updated. During time steps when Doppler and

heading information are provided, the measurement vector is:

$$\mathbf{z}(k) = \begin{bmatrix} \phi(k) \\ U(k) \end{bmatrix} \quad (4.4)$$

while during time steps when range measurements to one of the two transponders are provided, the measurement vector is:

$$\mathbf{z}(k) = \begin{bmatrix} r_1(k) \end{bmatrix} \quad (4.5)$$

or

$$\mathbf{z}(k) = \begin{bmatrix} r_2(k) \end{bmatrix} \quad (4.6)$$

as appropriate. The distances to the transponders, $r_1(k)$ and $r_2(k)$, are simply:

$$r_1(k) = \sqrt{(x_1 - x(k))^2 + (y_1 - y(k))^2} \quad (4.7)$$

$$r_2(k) = \sqrt{(x_2 - x(k))^2 + (y_2 - y(k))^2} \quad (4.8)$$

where (x_1, y_1) is the location of transponder 1 and (x_2, y_2) is the location of transponder 2.

For heading and speed measurement updates, the measurement model Jacobian $\mathbf{H}(k+1)$ is

$$\mathbf{H}(k+1) = \left. \frac{\partial \mathbf{h}(k+1)}{\partial \mathbf{x}} \right|_{\mathbf{x}=\hat{\mathbf{x}}(k+1|k)} = \begin{bmatrix} 0 & 0 & 1 & 0 \\ 0 & 0 & 0 & 1 \end{bmatrix} \quad (4.9)$$

Table 4.1: Kalman Filter parameters.

vehicle position process noise standard deviation	0.5 m
vehicle heading process noise standard deviation	0.2 deg
vehicle speed process noise standard deviation	0.05 m/sec
heading measurement noise standard deviation	2.0 deg
speed measurement noise standard deviation	0.05 m/sec
range measurement standard deviation	3 m

For beacon 1 updates,

$$\mathbf{H}(k+1) = \frac{\partial \mathbf{h}(k+1)}{\partial \mathbf{x}} \Big|_{\mathbf{x}=\hat{\mathbf{x}}(k+1|k)} = \begin{bmatrix} \frac{-(x_1-x(k))}{\sqrt{(x_1-x(k))^2+(y_1-y(k))^2}} & \frac{-(y_1-y(k))}{\sqrt{(x_1-x(k))^2+(y_1-y(k))^2}} & 0 & 0 \end{bmatrix} \quad (4.10)$$

For beacon 2 updates,

$$\mathbf{H}(k+1) = \frac{\partial \mathbf{h}(k+1)}{\partial \mathbf{x}} \Big|_{\mathbf{x}=\hat{\mathbf{x}}(k+1|k)} = \begin{bmatrix} \frac{-(x_2-x(k))}{\sqrt{(x_2-x(k))^2+(y_2-y(k))^2}} & \frac{-(y_2-y(k))}{\sqrt{(x_2-x(k))^2+(y_2-y(k))^2}} & 0 & 0 \end{bmatrix} \quad (4.11)$$

For our post-processed missions, the parameters for the Kalman Filter are listed in Table 4.1. These parameters are determined by operational capabilities of the sensors and our knowledge gained from previous vehicle missions.

The vehicle position process noise standard deviation is due to currents, which add noise to the x and y positions. Based on testing, this is estimated to be 0.5 m. The vehicle heading and speed process noise standard deviations are assumed to be 0.2 deg and 0.05 m/sec, based on testing and assumed current effects.

The measurement noise standard deviation is set by the sensor accuracies. The heading measurement noise standard deviation is listed by the manufacturer to be 1.0 deg; we use a value of 2.0 deg to account for mounting errors and our knowledge of past vehicle navigation results. The speed measurement noise standard deviation is 0.05 m/sec due to the ADCP manufacturer specifications. Finally, the range measurement standard deviation is set to 3 m, based on empirical testing, the use of 12kHz transponders, and the 1000 m to 6000 m operating distances from the transponders.

The EKF is initialized with a REMUS SLOBNAV fix during post-processing. This

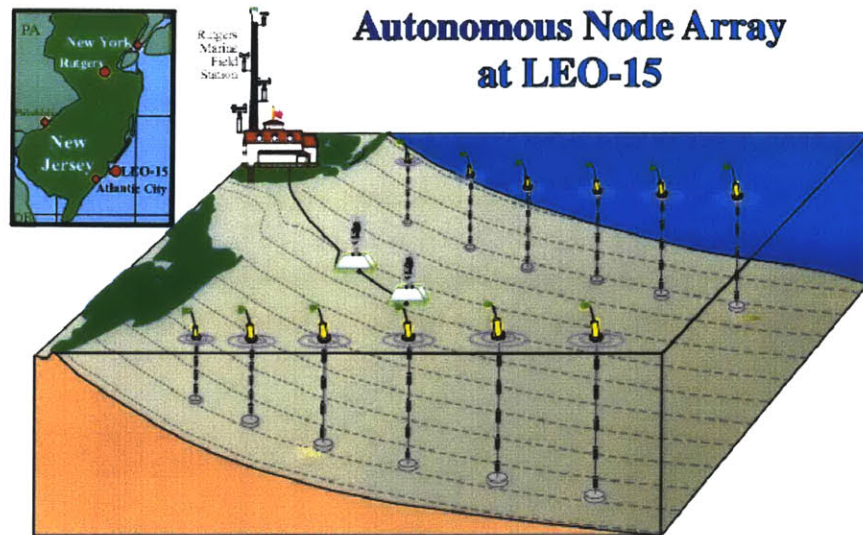


Figure 4-3: LEO-15 site as seen from the ocean bottom. The North line buoys are labeled N1-N6 from the shore, while the South line buoys are labeled A1-A6 from the shore, as shown in Figure 4-4. Each of the surface buoys and thermistor strings have a transponder positioned 5 meters from the surface for REMUS navigation. Note the permanent nodes in white, hard-wired to the field station. *Photo courtesy of Rutgers University.*

initialization assumes the REMUS fix is accurate within several meters. For the on-line mission, filter initialization is assumed to occur with a GPS fix, or by deploying the vehicle at a GPS verified transponder location.

4.2 Post-processed navigation missions - LEO-15, July 1999

Data from missions at the Longterm Ecosystem Observatory at a 15m depth (LEO-15) site in New Jersey was collected in July 1999. The LEO-15 site is seen in Figure 4-3.

The purpose of the LEO-15 initiative is to provide real-time, 24-hour presence in the ocean for data collection. The location in southern New Jersey was selected due to periodic up-welling events that occur there. Up-welling is a phenomenon where the warm surface waters are driven offshore and cold water is pulled from the ocean bottom to take its place. By taking constant oceanographic measurements, ocean forecasting, much like weather forecasting, can be done to predict future up-welling and physical events offshore. To continuously collect data, two nodes have been

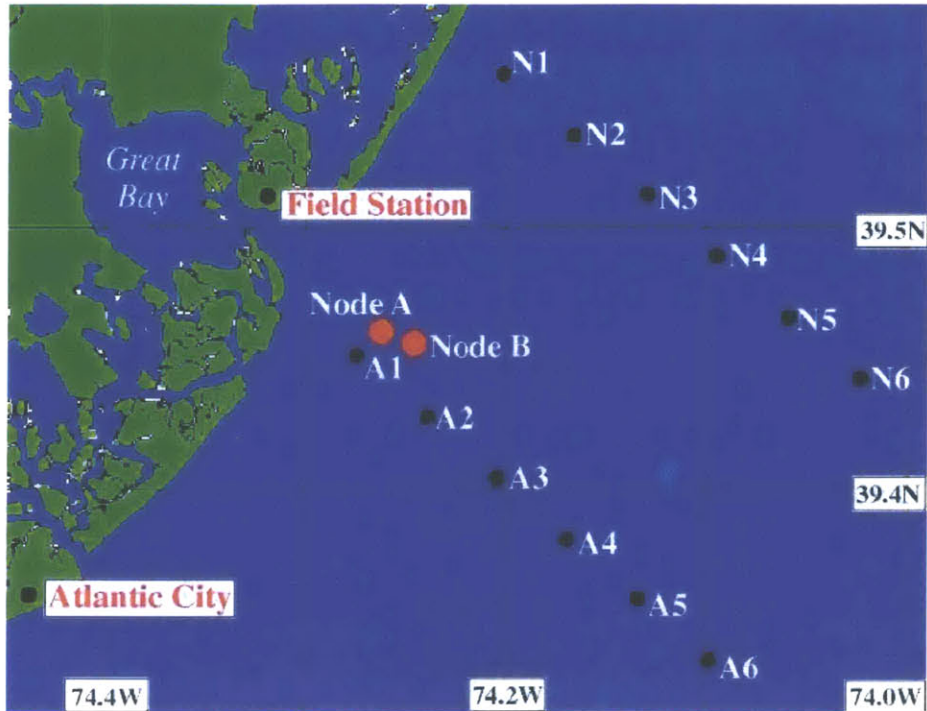


Figure 4-4: LEO-15 buoy lines showing location of line N1-N6 and A1-A6. The North line buoys are labeled N1-N6 from the shore, while the South line buoys are labeled A1-A6 from the shore. The REMUS missions used these transponders for LBL missions parallel to the 20 km buoy lines. The location of permanently fixed Nodes A and B, and the Field Station, are also provided. *Photo courtesy of Rutgers University.*

permanently mounted on the seafloor, measuring water temperature, salinity, clarity, wave height and period, chlorophyll content, and current speed and direction. The data from these nodes is augmented both with measurements from dedicated research vessels providing radiometers, CTD towed vehicles, and optical profilers, and satellites providing sea surface temperature, water quality and phytoplankton content [26].

There is an increase in up-welling episodes in the month of July. To examine this phenomenon, thermistor strings are added to the LEO-15 site. Comprised of several thermistors mounted on a line extending from the seafloor to a communication buoy on the surface, thermistor strings provide continual temperature recordings from set heights in the water column. This information produces detailed maps of the thermoclines in the area. As seen in Figure 4-3, these buoys are spaced 4km apart in a line from the shore.

The REMUS missions augmented this data collection in July 1998 by providing a mobile asset to map the water properties along the buoy lines shown in Figure 4-

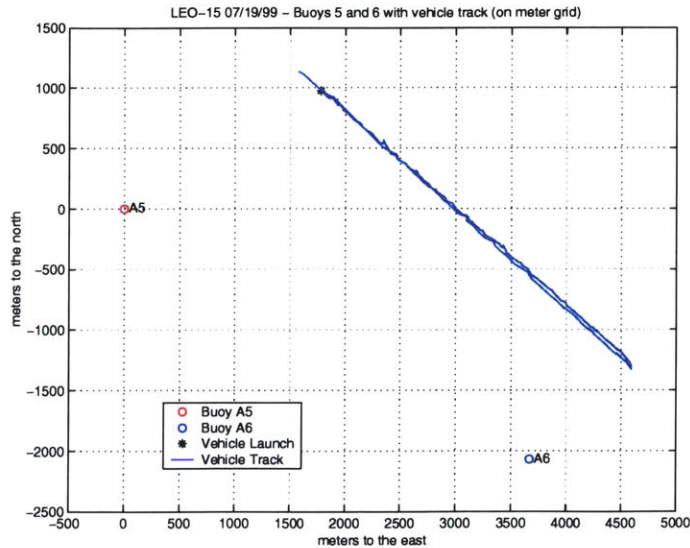


Figure 4-5: Vehicle trajectory for an 80 minute portion of an 8 hour REMUS LEO-15 mission, as plotted by the EKF. A5 and A6 designate the beacon locations. The first 7 minutes of this mission segment are analyzed in more detail in Figure 4-7 through Figure 4-20.

4. The vehicle’s task was to run 20km legs perpendicular to the beach, collecting Conductivity, Temperature, and Depth (CTD) information. These missions often exceeded 15 hours and 70km of continuous data collection.

As described in Chapter 3, REMUS navigates via LBL using two transponders at a time [28]. That is, in the first leg, buoys 1 and 2 are used; the second leg, buoys 2 and 3 are used, and so forth until the vehicle turns around at buoy 6, then the process is reversed. For post-processing, we examined a mission that was performed on July 19, 1999. The portion of the mission we looked at was at the end of the outbound leg, from Buoy 5 to Buoy 6, and the start of the inbound leg, from Buoy 6 to Buoy 5. This track is seen in Figure 4-5, and is indicative of the whole mission track. As shown in this Figure, the vehicle runs from Buoy 5 to Buoy 6, turns around, and repeats this track in the opposite direction, heading in toward shore.

4.2.1 Outliers

Any LBL mission will have outliers - range measurements that are incorrect. These are due to multipath, incorrect identification of the first acoustic arrival time, vehicle noise, or processing errors. If these outliers are taken as true range measurements,

the result will be a very 'jumpy' vehicle track, where the vehicle searches for the correct path through the water, chasing outliers. This searching track is undesirable due to the increased power consumption associated with the constant maneuvering. The searching track also does not allow the vehicle to follow a straight-line, yielding poor side-scan data or holidays in the vehicle coverage.

Figure 4-6 shows the ranges from buoys 5 and 6 for a 80 minute portion of the mission. We can see relatively steady returns, and our eyes can intuitively choose which range values are correct. We also see periods of outlier receipt, which are suspect. In this thesis, we examine two parts of this mission portion, then the mission as a whole. First, we focus on a 7 minute portion at the beginning of the interval (0 to 450 seconds) to study outliers and spurious measurements. Second, the section from 4400 to 5400 seconds is post-processed to examine extended acoustic dropouts. Period 0-450 will be discussed below, while period 4400-5400 will be discussed in section 4.2.4. Finally, the entire mission is examined in overview.

The key in Figure 4-6 and Figure 4-7 shows three separate measurements: `rangeraw`, `rangeunique`, and `rangeremus`. These three categories are the result of REMUS SLOBNAV methods and the need to classify the data as 1) new, unique ranges, 2) ranges passed from a previous timestep, or 3) ranges accepted by REMUS as 'reasonable', or believable measurements. First, `rangeraw` refers to all the measurements REMUS logs, which includes all new, passed, and REMUS accepted ranges. REMUS accepted ranges mean those that have passed SLOBNAV tests for reasonable and believable range measurements. Secondly, `rangeunique` includes all the new measurements (not passed from previous steps), before any tests to deem whether they are acceptable for use. Thirdly, `rangeremus` is the most exclusive range group, and includes measurements that are new ranges which REMUS has deemed acceptable by its measurement acceptance method, described in section 3.2.

To get a better view of the outliers from the 0-450 second period, Figure 4-7 shows the first 7 minutes of the mission between buoys 5 and 6. Differences of 100m are seen, which represents a 1.5% error in travel time of the acoustic signal.

1. Outlier Rejection Methods

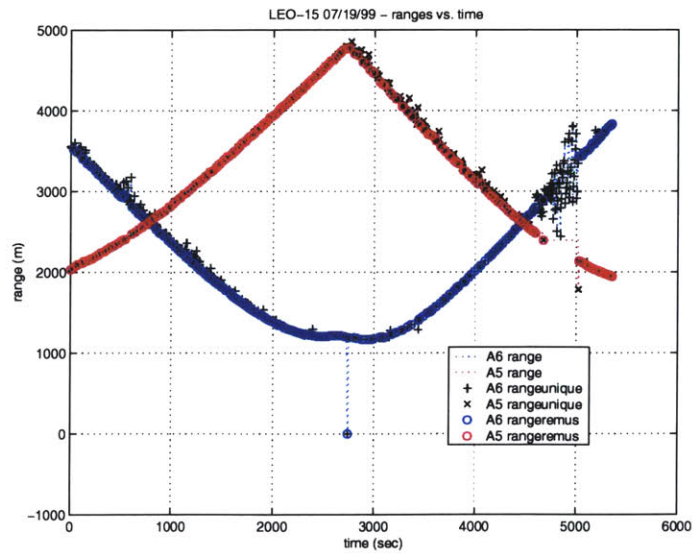


Figure 4-6: Range returns from buoys 5 and 6 for a 80 minute portion of mission. Note outlier acoustic returns 'jumping' off line of expected returns. A5 and A6 designate the beacon locations.

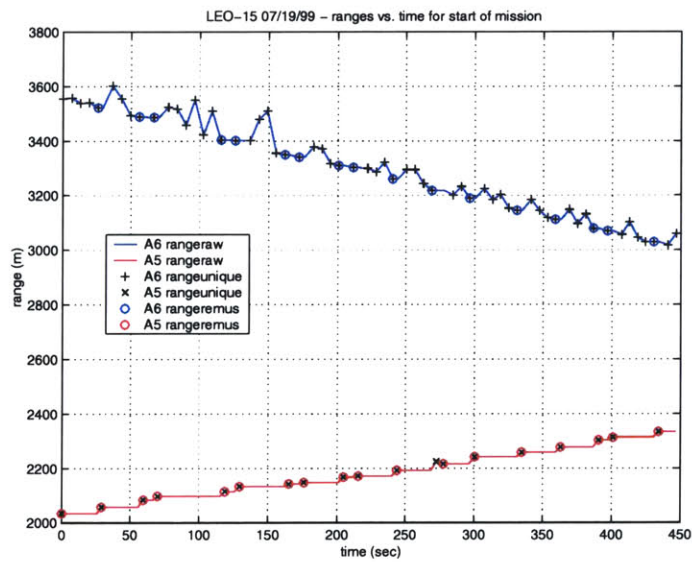


Figure 4-7: Range returns for 7 minute portion of mission. Note outliers of up to 100m from expected return.

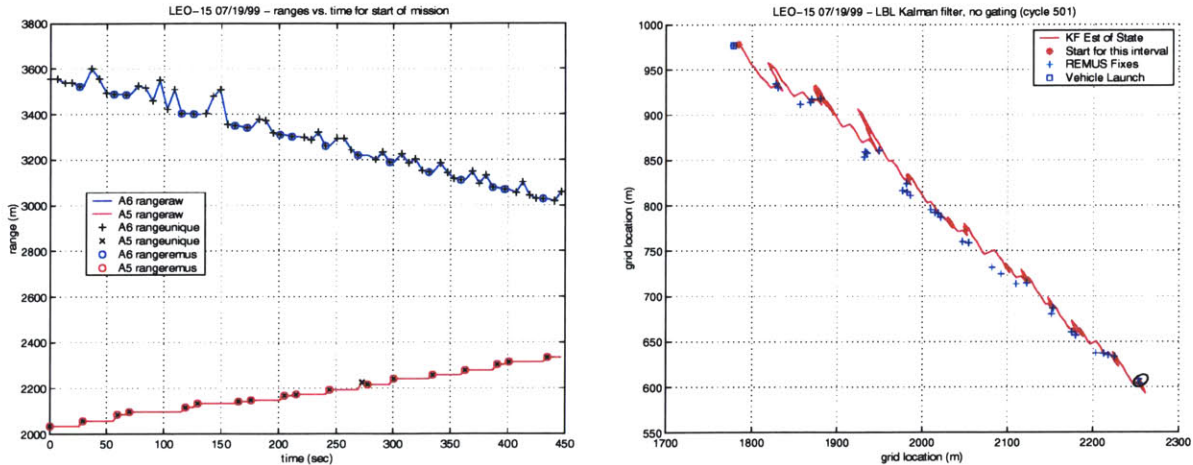


Figure 4-8: *Left*, Using all the range measurements for navigation (*i.e.*, without gating). *Right*, Yields a jumpy track that believes too many of the acoustic returns.

Two categories of outlier rejection are possible: time domain gating and spatial domain gating [31]. The difference between the methods is that time domain gating looks at each individual range measurement as it arrives, and spatial domain gating looks at the fix resulting from more than one measurement. These methods are more fully explained below.

The time domain method examines each measurement upon receipt, and determines whether that measurement is accurate based on comparison with the expected return time (or expected range of the transponder). If the measurement is deemed inaccurate, it is discarded and the next measurement is observed. This method allows for the immediate use of the measurement to update the EKF and the vehicle state, as there is no need to wait for the other beacon's range information to be recorded.

Spatial domain outlier rejection techniques compute a position fix and then attempt to determine if the fix is accurate based on the distance between the new fix and the previous vehicle position estimate. If the fix is inaccurate, the fix is discarded and new range measurements are processed. This method relies on the accuracy of both transponder returns to update vehicle position. If one range measurement is inaccurate, the vehicle continues to dead reckon without using the information gained from one accurate range measurement.

If measurements are accepted without an outlier rejection method, a jumpy, questionable track results. Figure 4-8 shows this case. All measurements are accepted as

accurate ranges to the transponders, including 100 m errors seen with the eye. This translates to a jumpy track, where the vehicle state is constantly reset by inaccurate ranges. Figure 4-8 shows the classic multipath example: instead of identifying the direct path acoustic return, a multipath return is identified. This results in a range that is longer (the acoustic signal arrives later) than the correct range. The vehicle track, then, is constantly reset back further than it actually is as it travels toward the transponder delivering the incorrect range information.

4.2.2 Gating

While the spatial domain outlier rejection techniques need both transponder ranges before determining if the measurements are valid, the time domain techniques allow us to validate and use the beacon measurements singly, upon arrival. Capitalizing on this benefit, we use a standard time domain method of gating, described by Vaganay *et al.* [30, 10], to discard outliers upon receipt. This gate compares the normalized innovation squared with a threshold γ [4, 30]:

$$\nu^t(k)\mathbf{S}^{-1}\nu(k) < \gamma \quad (4.12)$$

where the innovation

$$\nu(k) = z(k) - \hat{z}(k) \quad (4.13)$$

is the difference between the predicted and the measured range to the transponder, and

$$\mathbf{S}(k) = \mathbf{H}(k)\mathbf{P}(k+1|k)\mathbf{H}(k)^T + \mathbf{R}(k) \quad (4.14)$$

is the innovation covariance. Here, $\mathbf{H}(k)$ is the travel time Jacobian, $\mathbf{P}(k+1|k)$

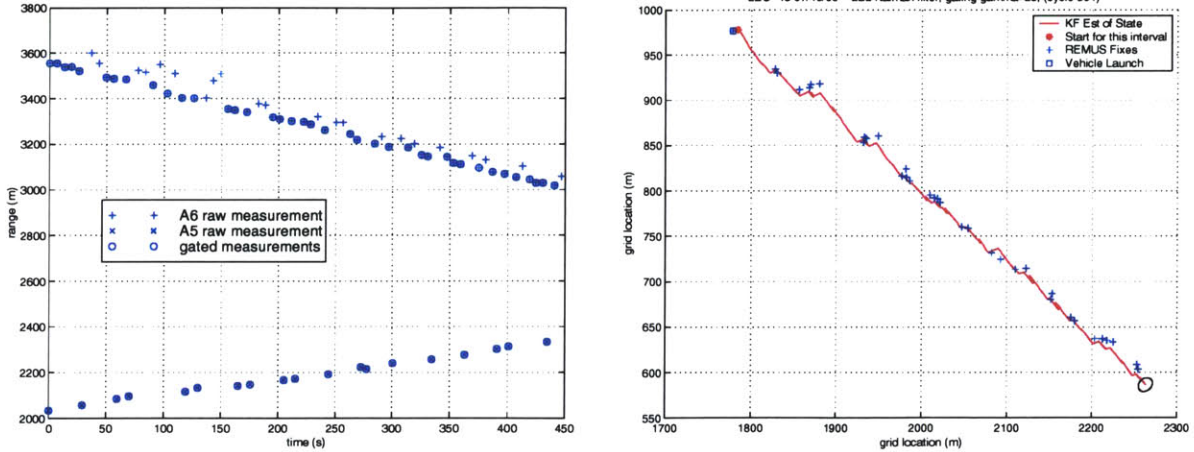


Figure 4-9: *Left*, Using gated range measurements with γ set to 25, we see the outliers from buoy 6 dropped from the navigation data set. *Right*, This gating of the ranges yields a smooth track which supplies an accurate representation of the vehicle mission trajectory.

is the covariance of the predicted vehicle position, and \mathbf{R} is the measurement noise covariance. Validated measurements are then used in the estimation step of the Kalman Filter to correct the current predicted position.

Setting $\gamma = 25$, we see in Figure 4-9 a much improved vehicle track over the case without gating. The outliers for Buoy 6 are excluded from the data set, where we see 36% (22 of 61 ranges) of the acoustic data rejected. Buoy 5, which seemed to have less of a problem with multipath and outliers, has none of the range measurements rejected. As seen in Figure 4-9, this yields a smooth, accurate vehicle track.

The γ gate is set for each mission, and depends on the same parameters that effect the frequency of outliers: acoustic properties leading to multipath, vehicle noise, and processing errors. The pitfall of this gating method is that too much data can be rejected by setting γ too low, leading to divergence. This method is particularly sensitive to divergence in a two beacon baseline, due to the lack of redundancy for fix information (*i.e.* two range circle intersects vice three or more intersects). The next section will explore the divergent case.

4.2.3 Divergence

As we mentioned in the previous section, the gate allows more or less measurements in to the filter, depending on how far they are from the expected return. We run

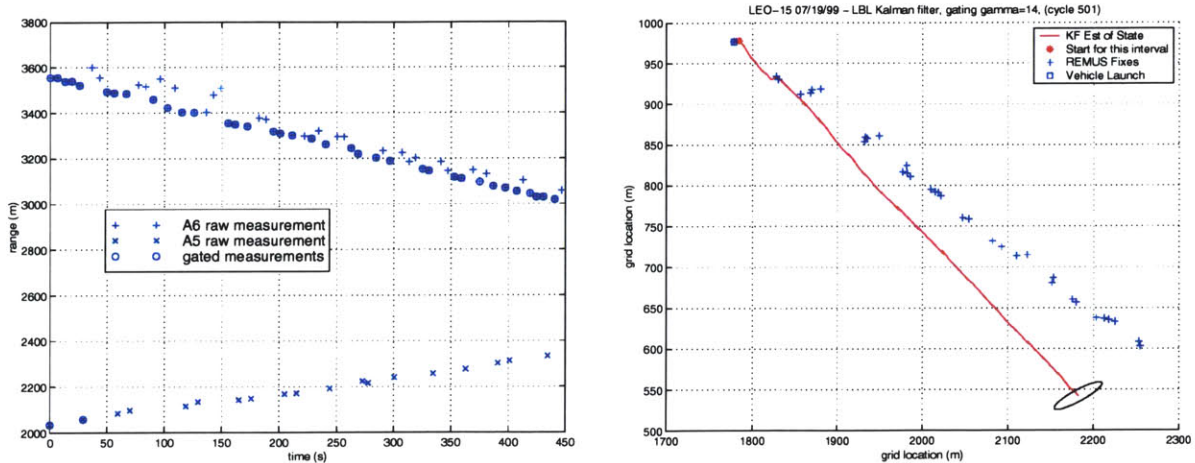


Figure 4-10: *Left*, Setting $\gamma = 14$, much of the Buoy 6 range measurements are rejected, while almost all of the Buoy 5 range measurements are rejected. *Right* This results in a diverging track and increased covariance.

the risk of discarding too much information, however, if we impose a narrow gate on the measurements. If a narrow gate discards information that could improve our navigation, the vehicle will dead reckon, and ultimately get lost. This condition leading to the position error growing without bound and the vehicle getting lost is called divergence of the navigation algorithm. The filter 'blows up', or position error increases without limit, resulting in no confidence in the vehicle position.

This sensitivity to divergence depends not only on the careful gating of measurements, but also on the geometry of the beacons. The most divergent-resistant case is three or more beacons that have ranges crossing at large angles to each other. In this case, one outlier will not affect the strong fix provided by the other beacons. In a two beacon arrangement as we have used, however, there is no backup information to provide a fix if the two beacons don't provide accurate measurements. Further, if the vehicle operates in an area where the beacon range spheres cross at a shallow angle, a small error in acoustic travel time can yield a large error in vehicle position. Therefore, the γ gate choice is very susceptible to divergence for a two beacon arrangement.

To illustrate the divergent case, we exhibit the example where $\gamma = 14$ in Figure 4-10. As this figure shows, $\gamma = 14$ is too narrow a gate for this mission, resulting in divergence. In this case, Buoy 6 had a 41% rejection rate for outliers, or 25 of 61

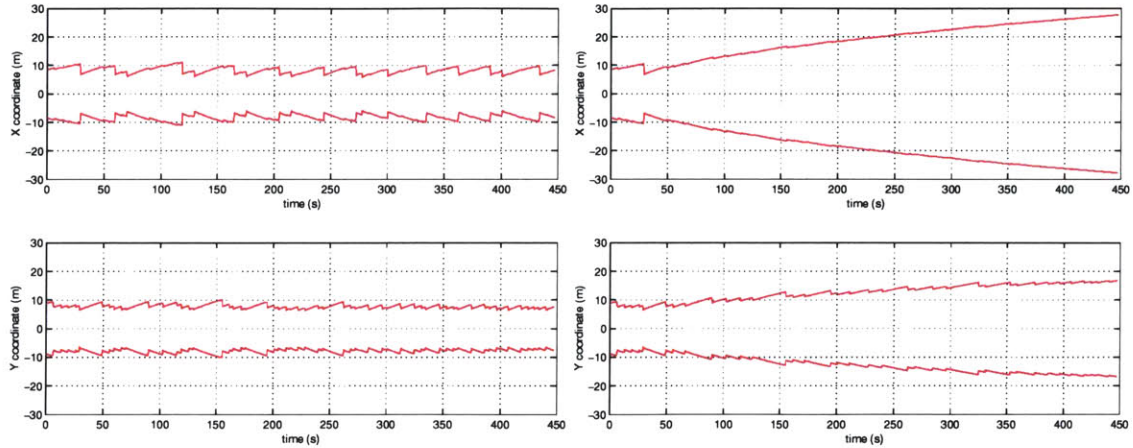


Figure 4-11: 3σ Position covariance for $\gamma=25$ (left) and $\gamma=14$ (right) for LEO-15 mission. measurements were ignored. Buoy 5, however, only accepts the first 2 measurements and rejects the rest, for a 89% rejection rate. The track shows initial good track following, then dead reckons for the rest of the mission due to the lack of information from buoy 5.

The divergence caused by rejecting too much measurement information is seen clearly as a growth in the error covariance by the end of this mission. Figure 4-11 shows the 3σ Position covariance for the two cases of $\gamma=25$ and $\gamma=14$. We see a 10m bound on uncertainty for the $\gamma=25$ case, due to the measurement updates to the vehicle position. For the $\gamma=14$ case, however, we see the unbounded growth on uncertainty due to no updates from buoy 5. The vehicle gets lost in the case where $\gamma=14$.

4.2.4 Extended acoustic dropouts

There may be periods of time during a mission when the acoustics do not yield a return, resulting in dropouts of minutes or longer. During our mission, this occurred in the time interval 4600-5000 seconds, or a 6 minute period, as seen in Figure 4-6. These dropouts have several different causes, such as shadow zones, turbulence, or topographical features blocking the transponder. When operating in a shadow zone or area of no transponder communication, the AUV is unable to obtain a range to that transponder.

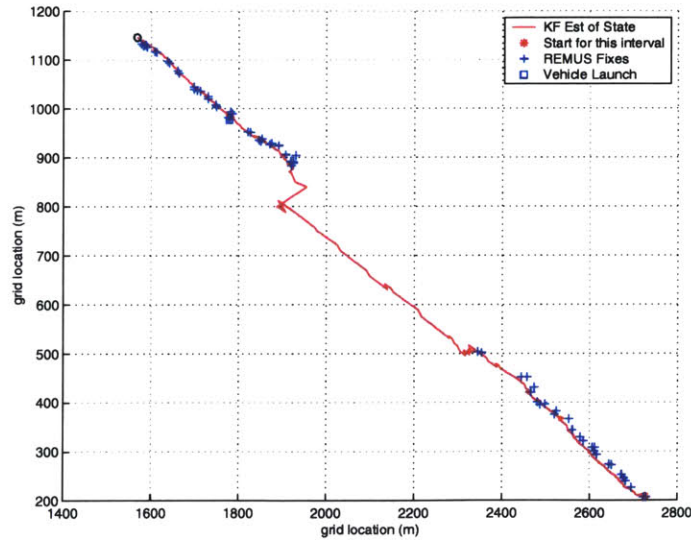


Figure 4-12: An extended acoustic dropout from time $t=4600$ to $t=5000$ seconds results in a lack of REMUS fixes for over 6 minutes during the mission.

In the case of a two transponder net, lack of range information from one transponder produces a gap in the vehicles navigation, as seen by the holiday in REMUS fixes in Figure 4-12. The vehicle is left to dead reckon during this interval.

The REMUS AUV experienced an extended acoustic dropout near the end of its inbound leg from buoy 6 to buoy 5, from 4600-5000 seconds. REMUS was unable to obtain a satisfactory return from buoy 6 in this interval, so it continued to interrogate that buoy until a satisfactory return was achieved. During this 6 minute period, REMUS continued to dead reckon its track, successfully in this instance.

By incorporating the EKF, a vehicle state is estimated for the period of the dropout. As seen in Figure 4-12, an estimate of the state is plotted in the break between fixes. This state provides an estimate of vehicle position during the lapse in acoustic fixes.

This example brings to light the requirement for a variable γ gate, which responds to the mission profile. During a period of extended acoustic dropouts, the measurement gate must grow with the state covariance. If the vehicle is unsure of its location, and the covariance grows, the measurement gate must increase to capture quality data as it's received. In the case from 4600-5000 seconds, we learn via post-processing that $\gamma=64$ (or 8 standard deviations from the mean of a bell-shaped standard distribution)

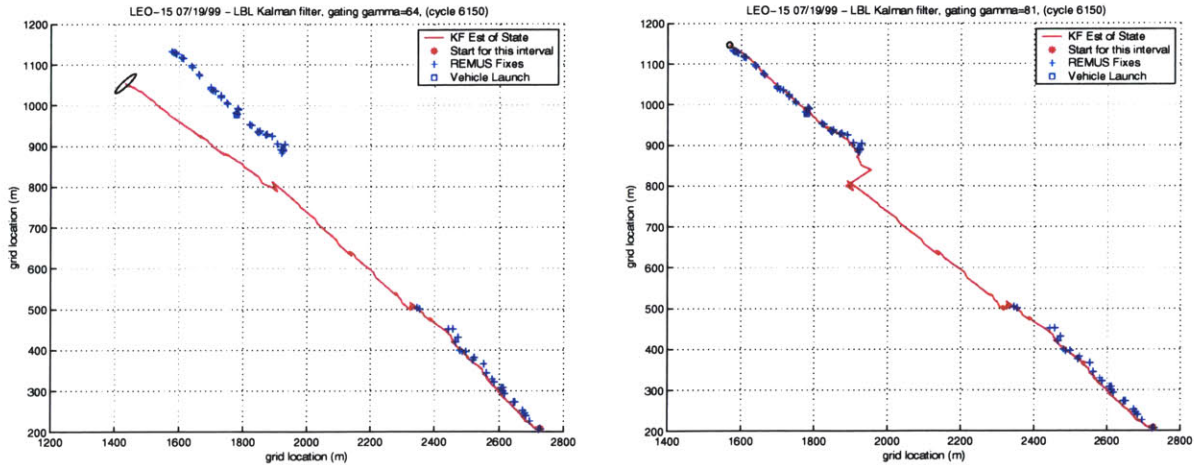


Figure 4-13: *Left*, Using gated range measurements with γ set to 64, we see the divergent track of the AUV due to the restrictive gate. *Right*, Using γ set to 81, conversely, yields a track that regains acoustic fixes.

leads to divergence, while $\gamma=81$ (or 9 standard deviations) leads to efficient gating and recovery of the navigation solution.

These two cases, $\gamma=64$ and $\gamma=81$, are shown in Figure 4-13. These vehicle trajectories reiterate the importance of a variable γ on the vehicle, responding to the confidence of the vehicle location.

The gated measurements for both the divergent and successful cases are seen in Figure 4-14. For both cases, we see that 100% of the ranges to buoy 5 are accepted before time $t=4600$ seconds. The difference between the two gate values is seen after $t=4600$. For $\gamma=64$, 26 of the next 27 measurements, or over 96%, are rejected for buoy 5. The gate is too small, and this quality data is discarded. Conversely, when the gate is set to $\gamma=81$, only 2 of the 27 measurements, or over 8%, are rejected. The gate is sufficiently large to accept the quality data, and results in a robust EKF with bounded error covariance growth.

The error covariance for both cases of $\gamma=64$ and $\gamma=81$ are seen in Figure 4-15. The divergent case of $\gamma=64$ shows an unbounded growth of the state estimate uncertainty after $t=4600$. When $\gamma=81$, we similarly see a growth in uncertainty after $t=4600$, but then a decrease and bounding of the error upon receipt of range information from both buoys at $t=5100$.

For the covariance graphs, note how the error in the y coordinate grows more

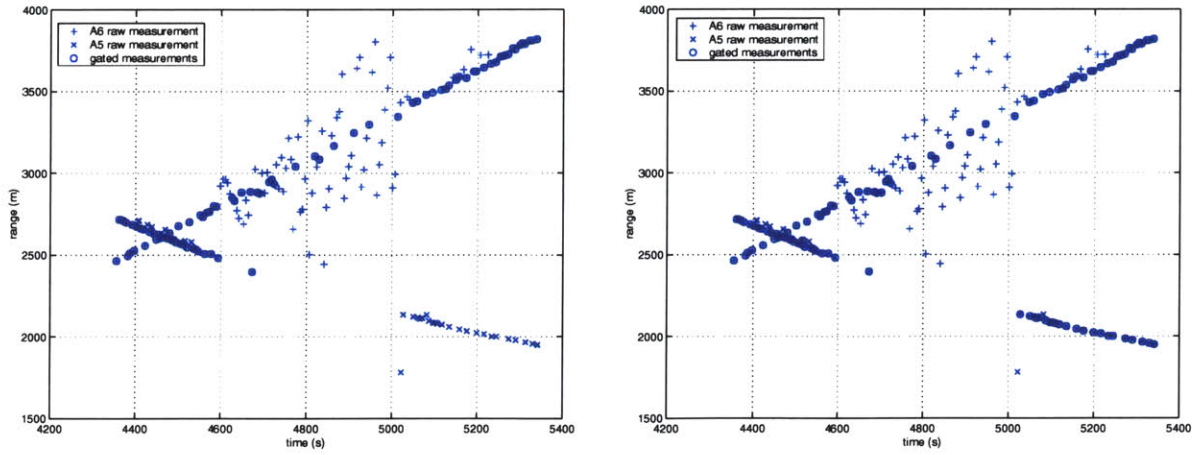


Figure 4-14: *Left*, Using gated range measurements with γ set to 64, 96% of buoy 5 range information is rejected after $t=4600$ seconds. *Right*, Using γ set to 81 yields an 8% rejection rate.

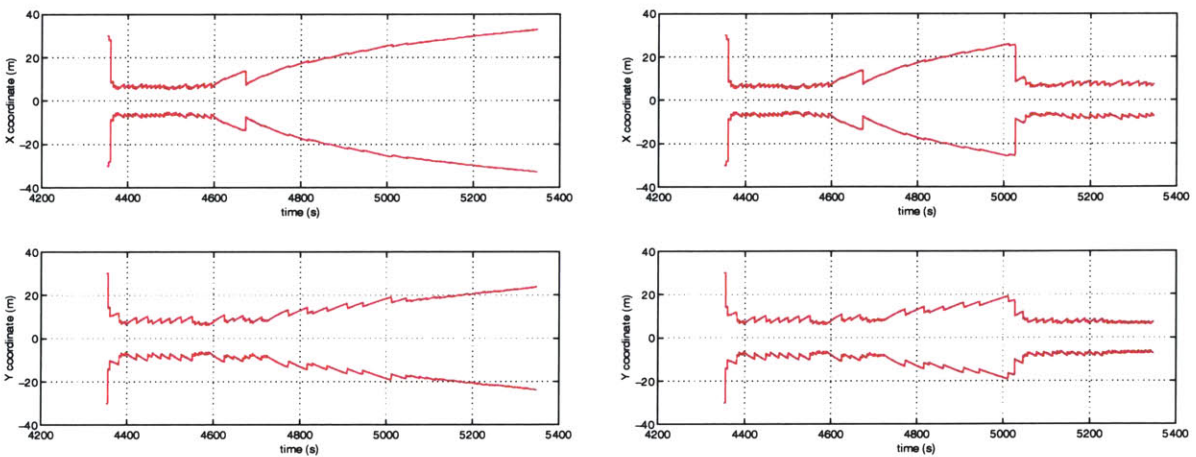


Figure 4-15: 3σ Position covariance for $\gamma=64$ (left) and $\gamma=81$ (right) for LEO-15 mission.

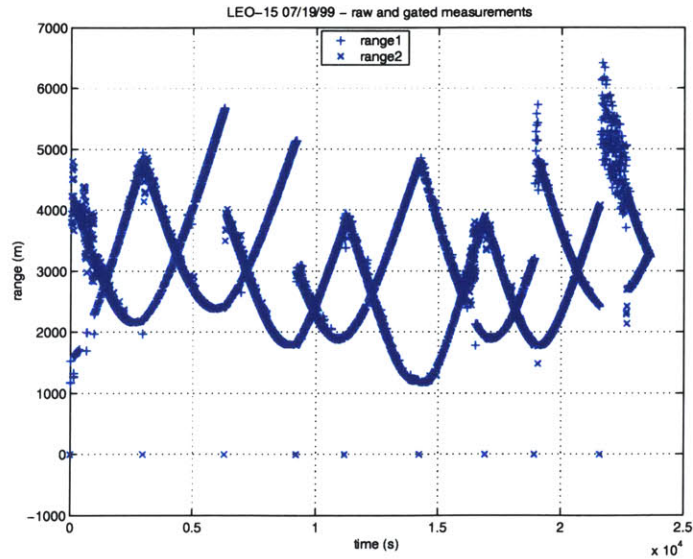


Figure 4-16: Range returns for complete LEO-15 mission 7/19/99. Outliers are evident around the cyclic transponder returns.

slowly than the error in the x direction. In this interval, the geometry of the range circles and vehicle location causes buoy 6 to provide more information for the y position than the x position of the vehicle. Conversely, buoy 5 offers most of the x position information, resulting in the rapid growth of uncertainty in this coordinate due to lack of buoy 5 information.

4.2.5 Complete mission post-processing

The complete mission was post-processed to test the robustness of the EKF. The acoustic returns shown in Figure 4-16 exhibit periods of spurious measurements, as described in section 4.2.1. In this section, we examined in detail the period from 12,000 seconds and 17,000 seconds, or from buoy 5 to 6, and returning from 6 to 5. This period is indicative of the mission profile, with cyclic transponder returns and outliers.

We first post-process the mission using $\gamma=25$, as shown in Figure 4-17. Here, we see the filter tracking the mission line from Buoy 1 to 6, then becoming lost on the return leg near Buoy 5. This agrees with the condition we have previously shown in Figure 4-9 and Figure 4-13. The filter navigates on the outbound leg satisfactorily, but diverges on the inbound leg near Buoy 5.

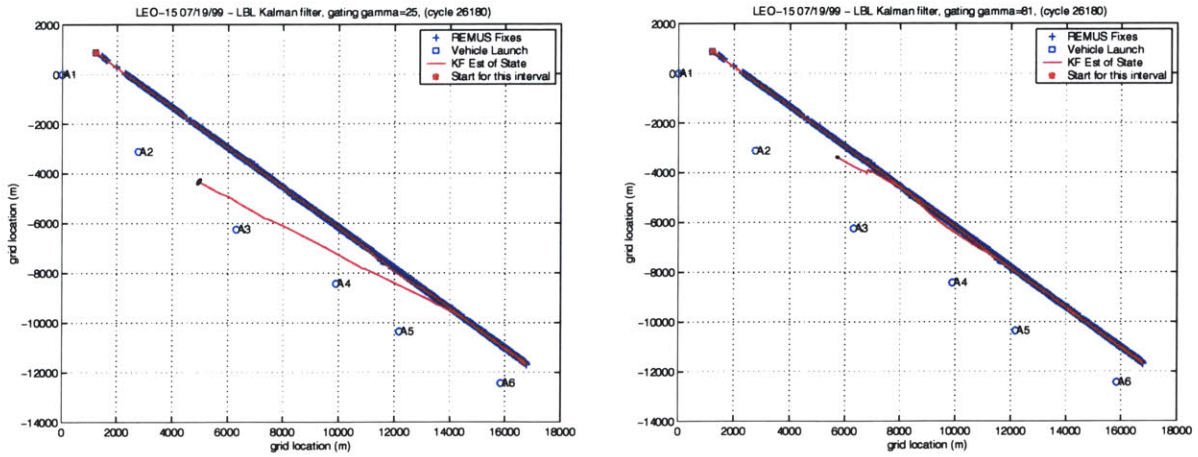


Figure 4-17: *Left*, Using gated range measurements with γ set to 25, we see the vehicle getting lost near Buoy 5. *Right*, Using γ set to 81 allows the vehicle to navigate beyond Buoy 3, at which point the navigation algorithm fails.

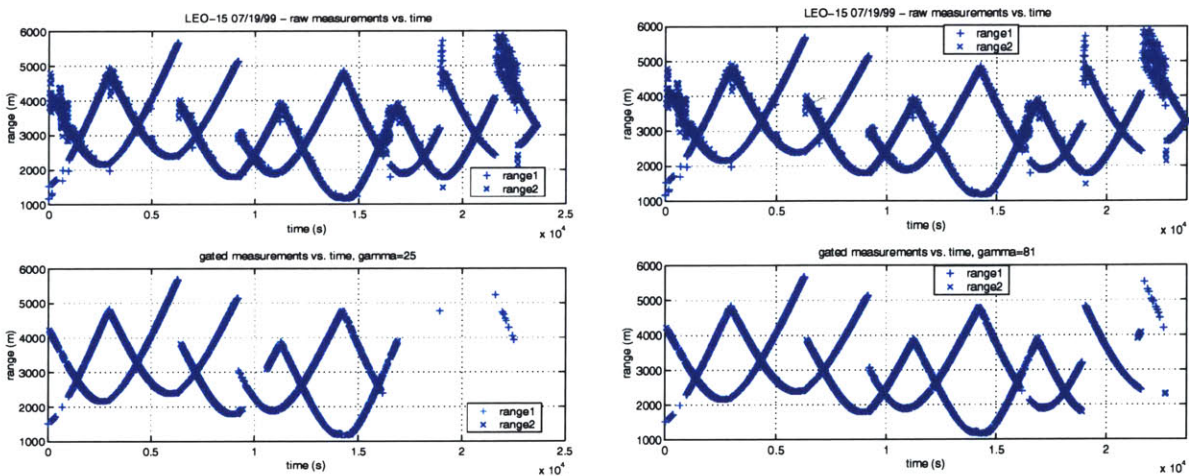


Figure 4-18: *Bottom Left*, Gated range measurements with γ set to 25. *Bottom Right*, Gated range measurements with γ set to 81.

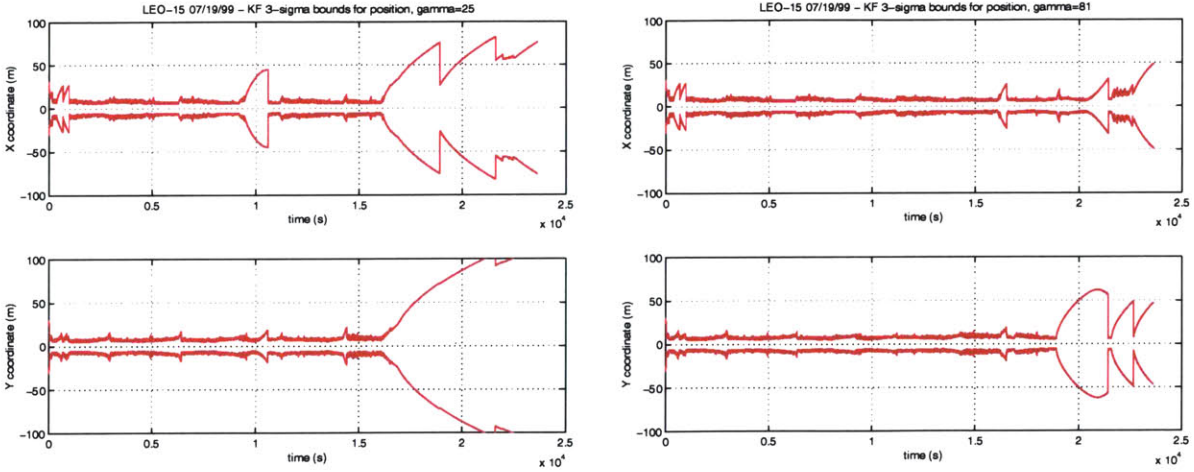


Figure 4-19: *Left* 3σ Position covariance for $\gamma=25$ and *Right* $\gamma=81$ (right) for LEO-15 mission.

When we use $\gamma=81$ in the post-processing, the vehicle navigates beyond Buoy 5, but is unable to utilize the range information from Buoy 2 at time 22,000 to 23,000 seconds. As seen in Figure 4-17, the EKF diverges and the vehicle loses the track.

The gated ranges for both cases of $\gamma=25$ and $\gamma=81$ are shown in Figure 4-18. The higher gating value permits more ranges to be utilized by the filter, and the vehicle navigates more robustly. The improved algorithm behavior is further seen in the decreased error covariance for $\gamma=81$, as seen in Figure 4-19.

4.3 Post-processing summary

We have shown in this section that the EKF used to post-process navigation data can yield a vehicle track with a position estimate between fixes. We have also seen how outlier rejection improves the navigation data for a smoother, more accurate track. Finally, we have shown the pitfalls of the gating method where we cause the navigation algorithm to diverge due to setting the gate too low, discounting valuable range information. The cases described in sections 4.2.1 to 4.2.3 - Outliers, Gating, and Divergence, are summarized in Figure 4-20.

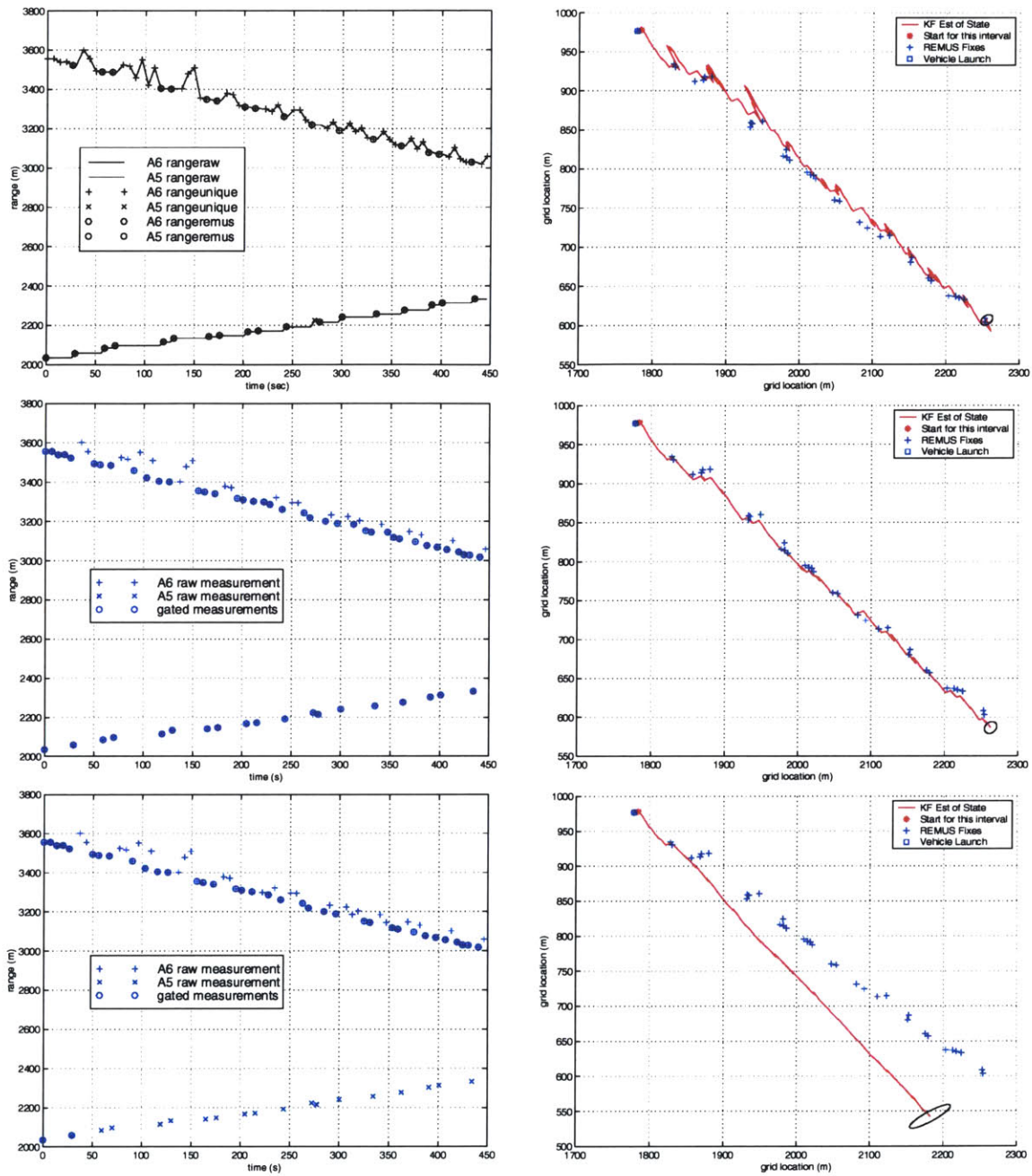


Figure 4-20: *Top left*, raw range measurements for LEO-15 mission segment. *Middle left*, gated range measurements for $\gamma=25$. *Bottom left*, gated range measurements for $\gamma=14$. With the lower value of γ , the filter accepts only the first two measurements from beacon 5. *Top right*, vehicle trajectory without outlier rejection. *Middle right*, vehicle trajectory for $\gamma=25$. *Bottom right*, vehicle trajectory for $\gamma=14$. With the lower value of γ , the filter accepts the first two measurements from beacon 5, resulting in divergence.

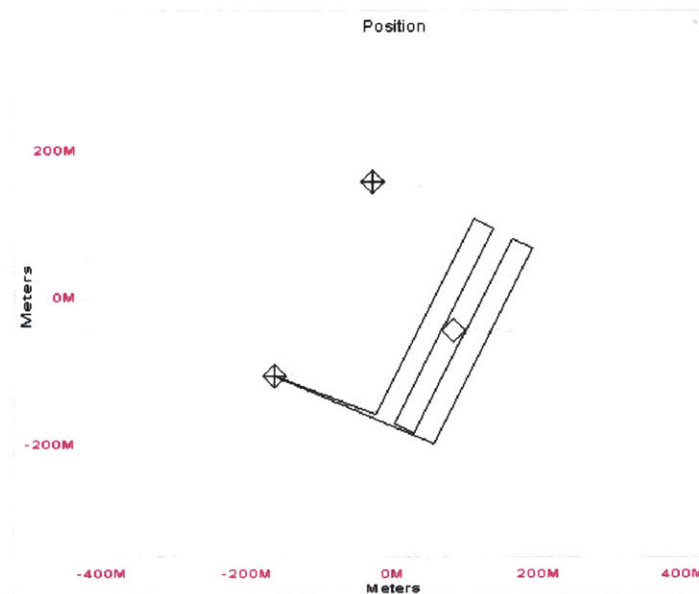


Figure 4-21: Vehicle mission profile as planned. Mini1 and Mini3 comprise the baseline. The vehicle starts at Mini1, then turns left and completes 4 rows of search about the shape marked with a square, then returns to Mini1.

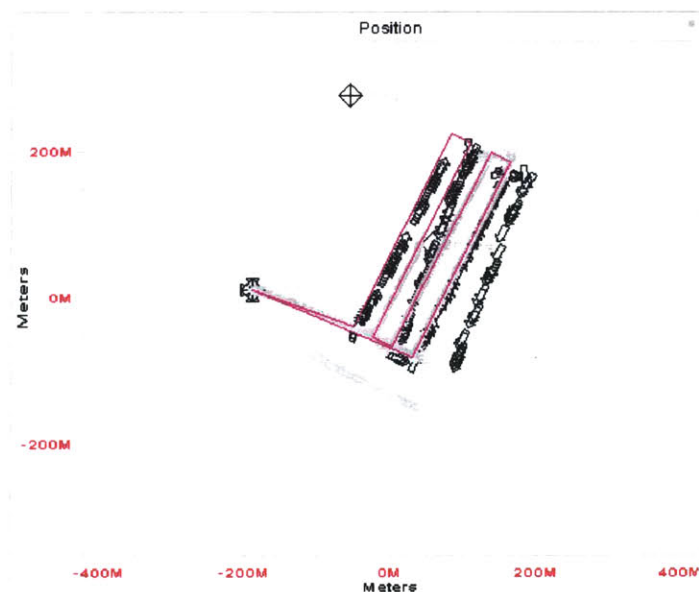


Figure 4-22: Vehicle mission profile as completed. The vehicle dead reckoned track is seen as small arrows on the planned route, while the acoustic fixes are marked with the big open arrows. Note the proper shape of the actual acoustic track, but the displacement due to dead-reckoning errors of the implemented Kalman Filter algorithm.

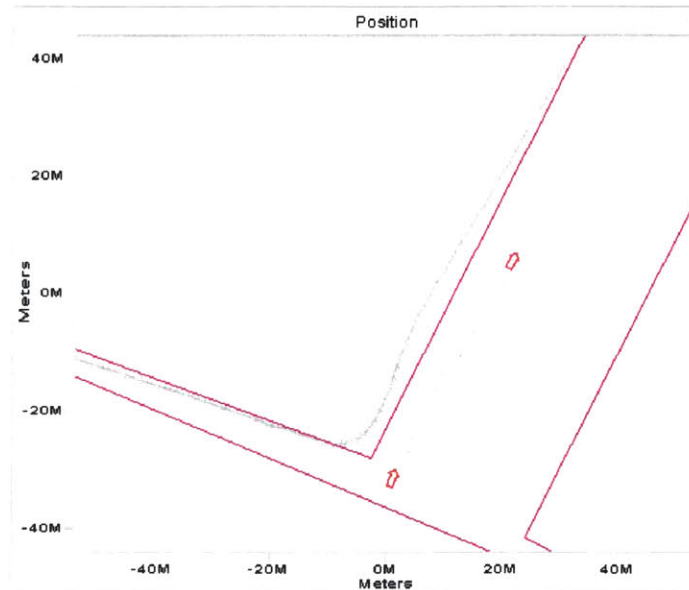


Figure 4-23: Detail of the first turn. Note the vehicle dead-reckoned to the first turn, then started acoustic fixes after the turn, noted by the large, open arrows.

4.4 On-line EKF missions - April 2000

In cooperation with the Woods Hole Oceanographic Institute Ocean Systems Lab, our EKF algorithm, written in Matlab, was converted to C language program code. Mr. Roger Stokey [28] completed this programming in April 2000. Real-time missions were then performed on April 18, 2000, in Buzzards Bay, Massachusetts. These results are seen in Figure 4-23 through Figure 4-28.

The mission profile was to traverse four evenly spaced rows, between two transponders labeled Mini1 and Mini2. This mission is typical of a shallow water side-scan sonar search mission. The planned mission is shown in Figure 4-21, and the completed mission is shown in Figure 4-22

During the on-line EKF mission, the vehicle was navigated by the EKF, with REMUS SLOBNAV navigation information saved to the disk. In each mission plot, the small arrows mark the Kalman Filter track, while the large outlined arrows mark the REMUS LBL fixes. The conversion to C language utilized some of the EKF Matlab code provided, and some of the existing SLOBNAV code. The result is a hybrid navigation system, controlled by the Kalman Filter using the gating of SLOBNAV. The end result is a navigation algorithm that dead-reckoned during the mission.

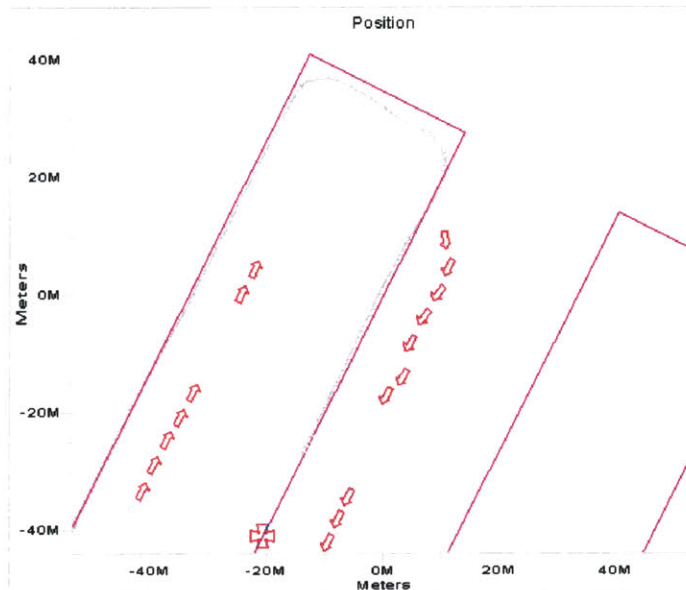


Figure 4-24: Detail of the second turn. Acoustic fixes are lost in the turn, then regained on the return leg.

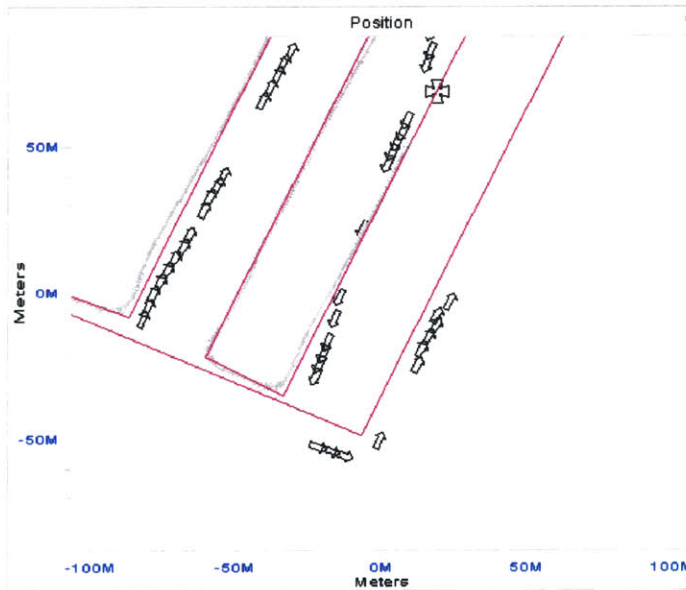


Figure 4-25: Detail of the third turn. Note how far the acoustic fixes are from the dead-reckoned track. Since the vehicle dead-reckoned for the length of the mission, these acoustic fixes did not correct the dead-reckoning errors.

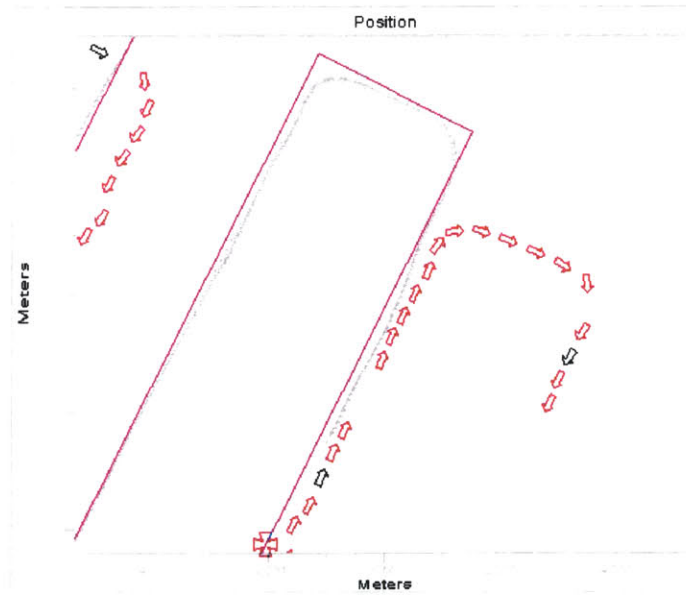


Figure 4-26: Detail of the fourth turn. The complete turn is seen with acoustic fixes, shifted to the right and down (East and South).

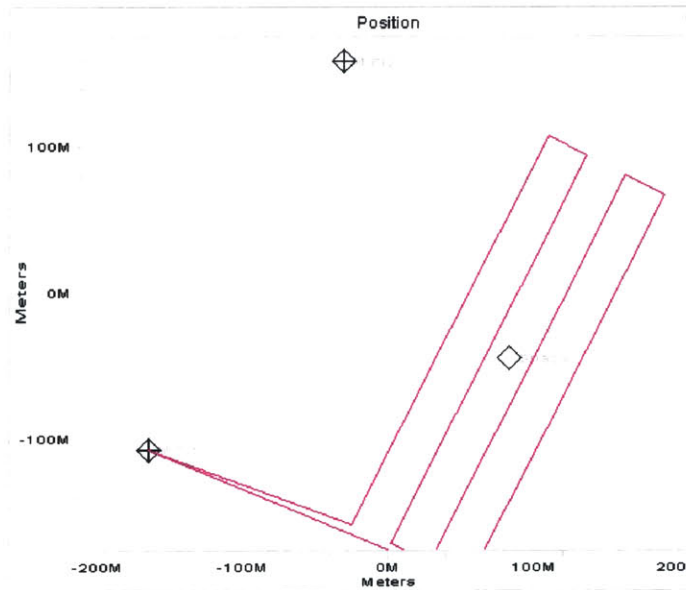


Figure 4-27: Close view of the vehicle mission profile as planned. Mini1 and Mini3 comprise the baseline.

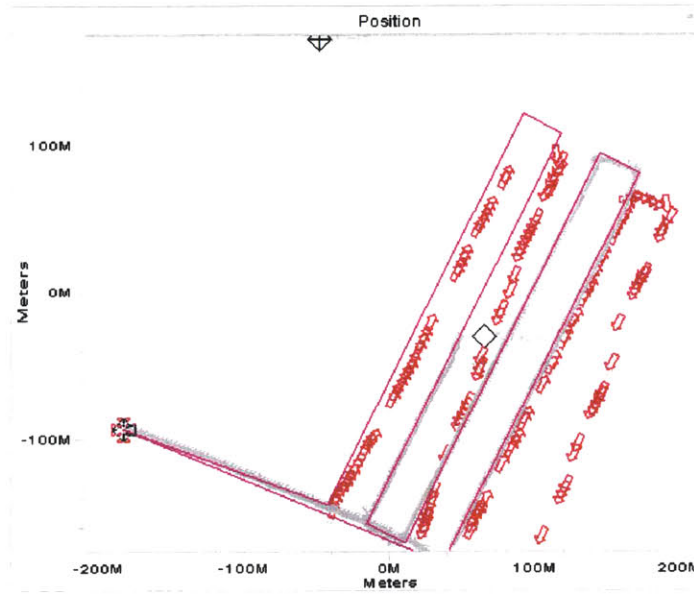


Figure 4-28: Close view of the vehicle mission profile as completed.

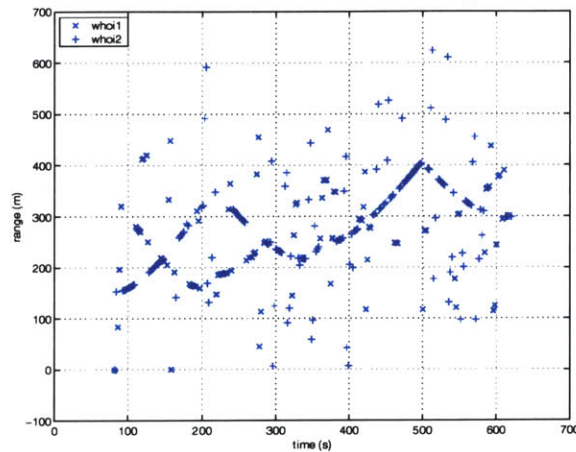


Figure 4-29: Raw acoustic returns from Mini1 and Mini2 show many outliers and multipath arrivals.

Post-processing the mission allowed us to apply our EKF directly to the acoustic data from REMUS. This also allowed us to try several gating values.

The acoustic data for the Buzzards Bay mission is shown in Figure 4-29. We see many outliers and multipath arrivals in this shallow water mission, where the depth was 3-4 meters. Though we can visually ascertain the correct arrival times of the repeating row mission profile, on-line gating of spurious measurements makes this a challenging navigation problem.

The mission was post-processed using a gate of $\gamma=1, 4,$ and 25 . These were chosen to graphically show the result of tuning the gate in the EKF.

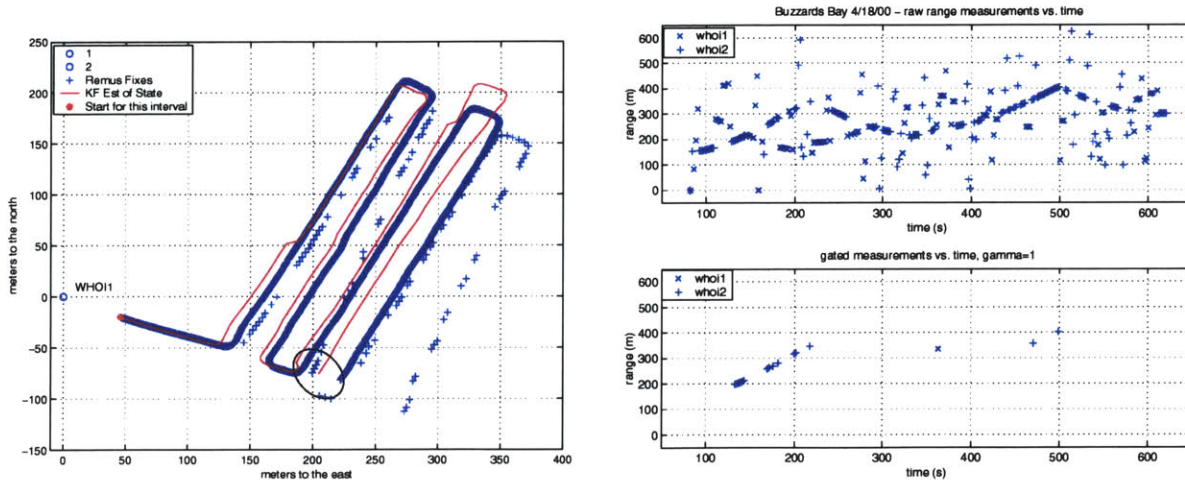


Figure 4-30: *Left*, Vehicle track with $\gamma=1$. *Right top*, Acoustic data showing all raw ranges, *Right bottom*, Gated ranges with $\gamma=1$ leads to a 94% rejection rate of acoustic returns.

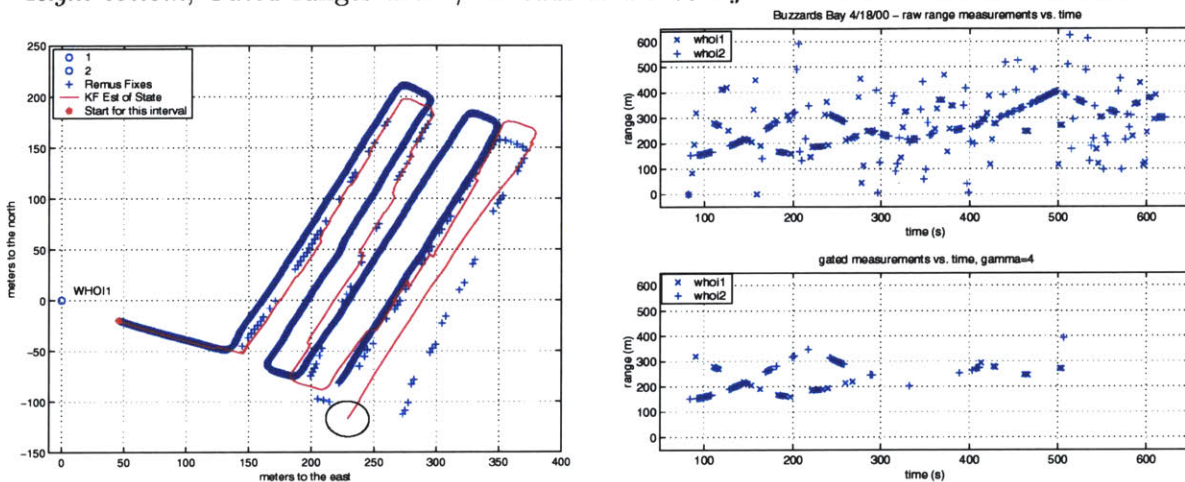


Figure 4-31: *Left*, Vehicle track with $\gamma=4$. *Right top*, Acoustic data showing all raw ranges, *Right bottom*, Gated ranges with $\gamma=4$ leads to a 68% rejection rate.

As seen in Figure 4-30, using a value of $\gamma=1$ leads to divergence of the filter. The filter dead reckons most of the track, due to a 94% rejection rate of the acoustic returns. Of the 249 ungated range returns, only 16 are accepted. This gate is too restrictive, throwing out range information that would assist the navigation algorithm.

Figure 4-31 exhibits the case of $\gamma=4$. The filter now accepts 77 of the 249 range returns, or a 68% rejection rate. This causes the EKF to track the vehicle path through time $t=280s$, after which the filter diverges. The acoustic return plot shows excellent filtering of the ranges before $t=280s$, then sporadic acceptance of the actual acoustic range returns. This results in divergence, as seen in the 3σ covariance plots

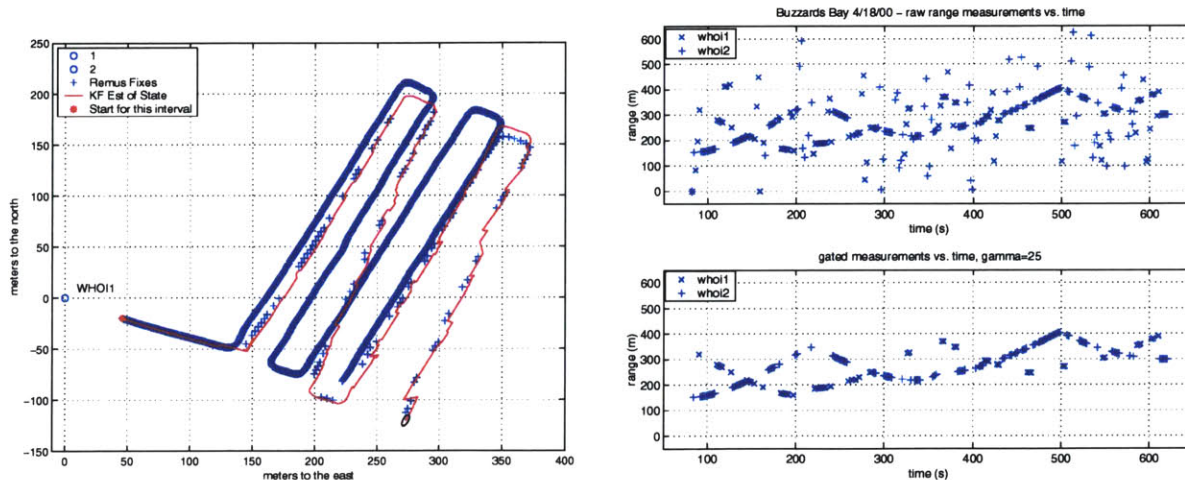


Figure 4-32: *Left*, Vehicle track with $\gamma=25$. *Right top*, Acoustic data showing all raw ranges, *Right bottom*, Gated ranges with $\gamma=25$ leads to a 37% rejection rate.

in Figure 4-33.

The filter performs very well when $\gamma=25$. This case is illustrated in Figure 4-32. We see excellent tracking of the REMUS fixes, 159 of the 249 acoustic returns accepted. The accepted ranges shown in Figure 4-32 show the coherent cyclic returns of a row mission between two transponders. The 3σ error covariance in Figure 4-33 shows a consistent 3m bound.

A summary of the post-processed Buzzards Bay mission is seen in Figure 4-33. This summary includes the error covariance from each case, illustrating how the covariance decreases as γ increases.

4.5 Extended Kalman Filter navigation summary

We have shown the ability of the EKF to navigate a mission via post-processing of acoustic data. We have also shown the sensitivity of a two-beacon LBL layout to EKF divergence. Because no absolute ground truth position information is available for the experiments that we have performed thus far, we are unable to determine the absolute accuracy of the navigation method at this time.

In independent experiments, Stokey has compared the accuracy of his fix-based position method with ground truth. He determined that the method is accurate to approximately three meters in shallow water with high frequency transponders [7].

The accuracy of his method is believed to be on the order of 5-10 meters when using low frequency transponders.

Figure 4-34 shows the fixes obtained by Stokey's method plotted with EKF fixes for the April 18 Buzzards Bay mission. Figure 4-35 shows the distance between the EKF positions and the REMUS fixes. The mean distance between the fixes is approximately 5 meters. For this reason, we believe that the EKF position estimates for the LEO-15 mission in this thesis are accurate to approximately 15 meters.

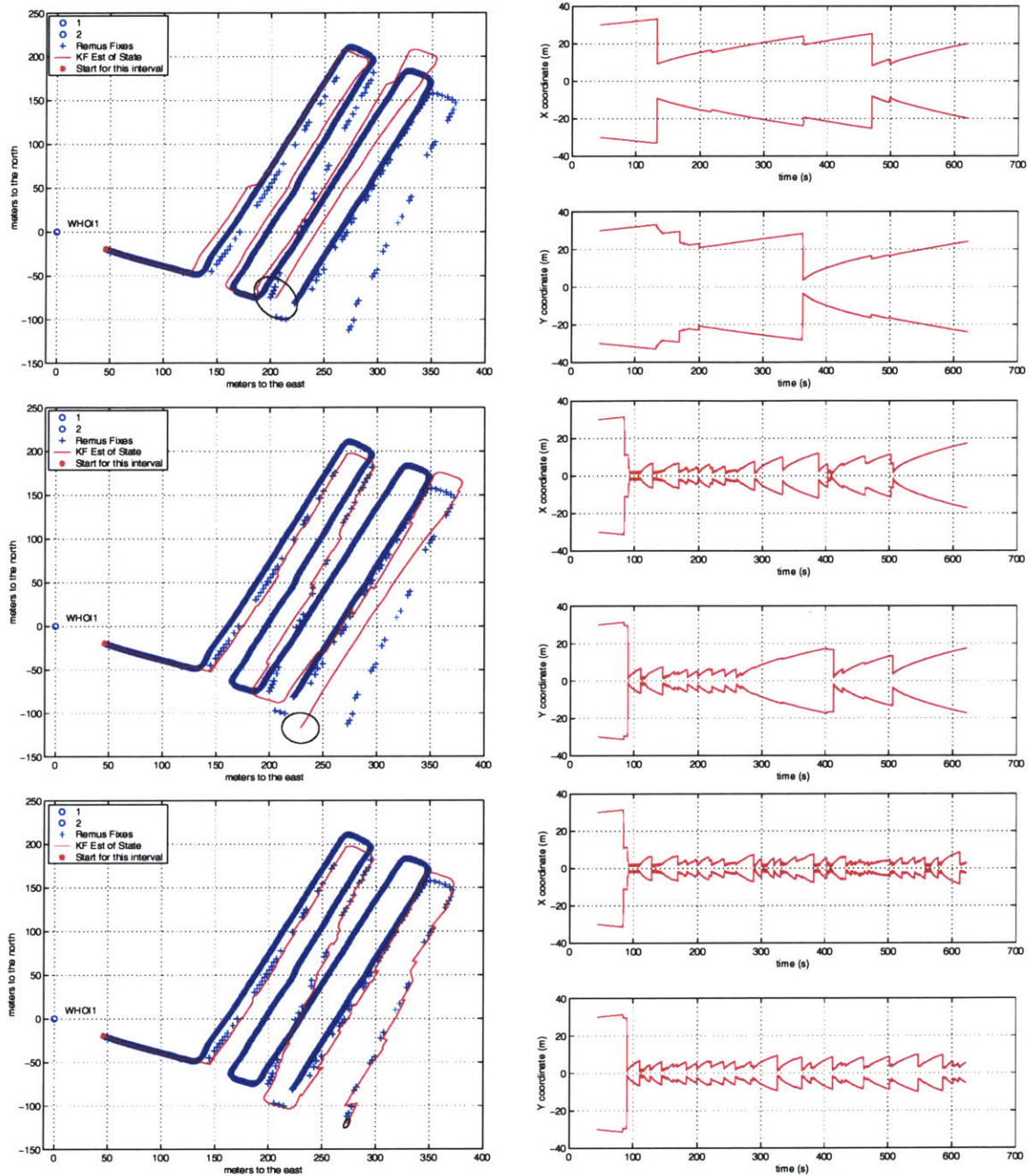


Figure 4-33: *Top left*, vehicle trajectory with $\gamma=1$. *Middle left*, vehicle trajectory for $\gamma=4$. *Bottom left*, vehicle trajectory for $\gamma=25$. As the value of γ decreases from 25 to 4 to 1, only 5% of the measurements are accepted, leading to a diverging navigation algorithm. *Top right*, 3 σ Position covariance for $\gamma=1$. *Middle right* Covariance for $\gamma=4$. *Bottom right*, Covariance for $\gamma=25$.

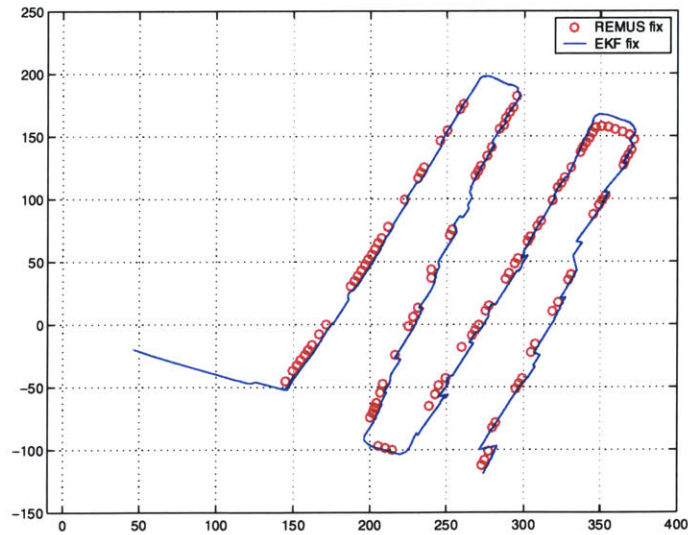


Figure 4-34: REMUS SLOBNAV fixes plotted with EKF fixes. We see the SLOBNAV fixes coincide well with EKF fixes.

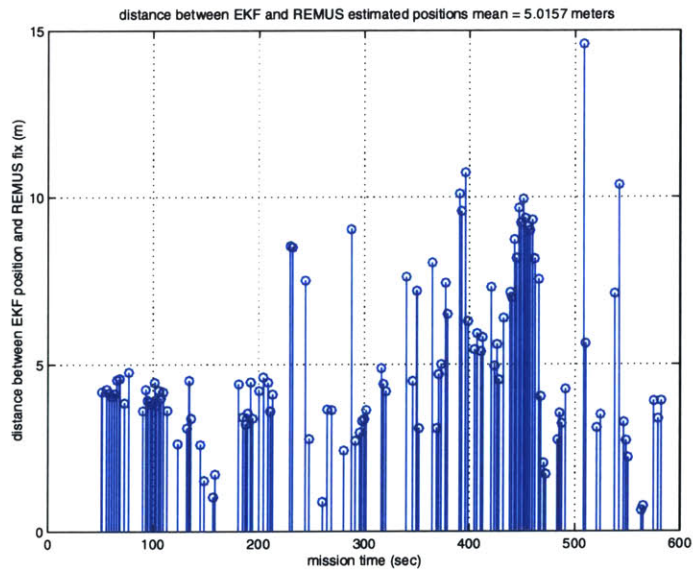


Figure 4-35: Step plot of position error between REMUS SLOBNAV fixes and EKF fixes show an accuracy of within 5 meters between the two methods.

Chapter 5

Conclusions

This thesis has investigated the implementation of the Extended Kalman Filter on the AUV REMUS. This chapter concludes the thesis by summarizing the contributions of the thesis research and making suggestions for future research.

5.1 Contributions

The contributions of the thesis have been the following:

- Navigation missions for the AUV REMUS were post-processed and evaluated using an EKF.
- An EKF has been implemented on the AUV REMUS
- The utility of the EKF has been assessed for a small, low-cost AUV.
- The limitations of the EKF in a two-beacon LBL net have been examined.

Via post-processing of navigation data, the utility of the EKF can be studied for a small, low-cost AUV. We have noted the effect of outlier rejection, and the sensitivity of the measurement domain gating to the gate value. This gate value has been shown to be a critical factor in the EKF navigating successfully, or leading to a diverging condition and the vehicle getting lost.

The limitations of the EKF are pronounced in a two-beacon LBL net. We have shown that the filter diverges quite readily if the gating is not appropriate for the mission. Poor gating is a critical problem if there are only two sources of acoustic data. If one transponder does not offer accurate ranges, the vehicle is left with only one source of data, and inevitably gets lost. By adding another range source, one transponder can offer poor accuracy, and the remaining transponders can continue to provide accurate ranges for the EKF.

The implementation of the EKF on the vehicle did not run flawlessly. In fact, the vehicle dead-reckoned for the EKF mission, as described in Chapter 4. Due to time constraints of the REMUS programmer, we were unable to have the vehicle be controlled by the EKF algorithm during a mission before the printing of this thesis. Our mission did provide useful data for post-processing, however, in a very cluttered, multi-path environment. The results of this EKF mission show both the quality of the SLOBNAV navigation method developed by WHOI OSL, and the ability of the EKF to handle such multi-path environments. The ability to reliably operate in the shallow water zone is impressive, and kudos are given to WHOI OSL for routinely carrying out these missions.

5.2 Future research

Future areas of research for improving the EKF lie in two principal areas:

1. Using a variable gate for outlier rejection
2. Implementing a hydrodynamic model of the REMUS vehicle in the plant model

These are examined in the following sections.

- **Variable gate for outlier rejection**

We have found that each mission portion has a gate which leads to optimal performance of the EKF navigation algorithm. By utilizing a variable gate for outlier rejection, we can tune the filter to the acoustic conditions of each

mission portion. In our post-processing examples of Chapter 4, we see that the outbound leg of buoys A5 to A6 utilized a gate of $\gamma=25$, and diverged when $\gamma=14$. On the inbound leg of the same buoy pair, the filter required a gate of $\gamma=81$ to provide a vehicle position, while $\gamma=64$ resulted in a diverging EKF. It appears a robust EKF should simply maintain a very large gate, to guard from divergence. This is not the case, as a large gate creates other problems in navigation. By setting γ to a very large value, too much information is accepted to update the filter, negating the value of a selective measurement gate.

The challenge is to identify the optimal gate during a real-time mission, which is robust enough to handle the myriad acoustic conditions encountered in the shallow water environment. The gate could be related to the confidence of each fix via a relation to the state covariance \mathbf{P} , increasing when \mathbf{P} increases, and decreasing when \mathbf{P} decreases. This would effectively widen the gate when there is a large state covariance, accepting more measurements due to the uncertainty in position. The gate would be smaller when the state covariance is small, indicating a high confidence in vehicle location.

- **Hydrodynamic model of the REMUS vehicle**

Implementing a hydrodynamic model of the REMUS vehicle offers the ability to improve calculation of the predicted state. By using REMUS hydrodynamics in the plant model \mathbf{F} , the predicted state will be based on REMUS specific motions, rather than a generic plant motion. Work toward this goal is being pursued by Prestero [24].

An accurate plant model, coupled with control surface input, offers the ability to dead reckon with greater accuracy. This development will allow the vehicle to navigate more precisely through acoustic dropout areas, where environment information is lacking. This promises a more robust navigation algorithm, relying on proprioceptive data as well as acoustic data.

Bibliography

- [1] B. Allen, R. Stokey, T. Austin, N. Forrester, R. Goldsborough, M. Purcell, and C. von Alt. REMUS: A small, low cost AUV; system description, field trials and performance results. *IEEE J. Ocean Engineering*, 1997.
- [2] W. Au. *The Sonar of Dolphins*. New York: Springer-Verlag, 1993.
- [3] J. Baker and H. Thomas. An integrated DGPS/acoustic system for underwater positioning. In *uust*, 1999.
- [4] Y. Bar-Shalom and T. E. Fortmann. *Tracking and Data Association*. Academic Press, 1988.
- [5] Y. Bar-Shalom and X. R. Li. *Estimation and Tracking: Principles, Techniques, and Software*. Artech House, 1993.
- [6] S. Beiter, R. Poquette, B.S. Filipo, and W. Goetz. Precision hybrid navigation system for varied marine applications. *IEEE Trans. Aerospace and Electronic Systems*, pages 316–323, 1998.
- [7] C. Cassidy. Navigation and target localization performance for underwater vehicle REMUS. Master’s thesis, Massachusetts Institute of Technology, May 2000.
- [8] I. J. Cox and G. T. Wilfong. *Autonomous Robot Vehicles*. Springer-Verlag, 1990.
- [9] T. Curtin, J. G. Bellingham, J. Catipovic, and D. Webb. Autonomous ocean sampling networks. *Oceanography*, 6(3):86–94, 1993.

- [10] H. J. S. Feder, C. M. Smith, and J. J. Leonard. Incorporating environmental measurements in navigation. In *IEEE AUV*, Cambridge, MA, August 1998.
- [11] T. Fulton, C. Cassidy, J. Leonard, and R. Stokey. Navigation sensor data fusion for the AUV REMUS. In *Symposium for Unmanned Robotics Technology*, 2000.
- [12] R. L. Greenspan. GPS and inertial navigation. In *Global Positioning System: Theory and Applications*, volume 2, chapter 7. American Institute of Aeronautics and Astronautics, 1996.
- [13] M. Hunt, W. Marquet, D. Moller, K. Peal, W. Smith, and R. Spindel. An acoustic navigation system. Technical Report WHOI-74-6, Woods Hole Oceanographic Institution, 1974.
- [14] Precision Navigation Incorporated. <http://www.precisionnav.com>, 2000.
- [15] A. Jircitano, J. While, and D. Dosch. Gravity based navigation of AUVs. In *Proceedings of the Symposium on Autonomous Underwater Vehicle Technology*, pages 177–180, Washington, DC, USA, June 1990.
- [16] M. Kuristky and M. Goldstein. Inertial navigation. In I. Cox and G. Wilfong, editors, *Autonomous Robot Vehicles*. Springer-Verlag, 1990.
- [17] J. J. Leonard, A. A. Bennett, C. M. Smith, and H. J. S. Feder. Autonomous underwater vehicle navigation. In *IEEE ICRA Workshop on Navigation of Outdoor Autonomous Vehicles*, Leuven, Belgium, May 1998.
- [18] E. Levinson and C. San Giovanni. Laser gyro potential for long endurance marine navigation. In *IEEE Trans. Aerospace and Electronic Systems*, pages 115–129. Sperry Gyroscopic Div, Great Neck LI NY 11020, 1980.
- [19] E. S. Maloney, editor. *Dutton's Navigation and Piloting*. Annapolis, MD: Naval Institute Press, 1985.
- [20] M. B. May. Gravity navigation. In *Record of the 1978 Position Location and Navigation Symposium*, pages 212–218, San Diego, CA, USA, November 1978.

- [21] P. Maybeck. *Stochastic Models, Estimation, and Control, vol. 1*. Academic Press, 1979.
- [22] P. H. Milne. *Underwater Acoustic Positioning Systems*. London: E. F. N. Spon, 1983.
- [23] J. G. Paglia and W. F. Wyman. DARPA's Autonomous Minehunting and Mapping Technologies (AMMT) Program: An Overview. In *IEEE Oceans*, pages 794–799, Ft. Lauderdale, FL, USA, September 1996.
- [24] T. Prestero. A description of the REMUS autonomous underwater vehicle. Oceanographic systems laboratory report, Woods Hole Oceanographic Institution, Woods Hole, MA, March 2000.
- [25] H. Schmidt, J. Bellingham, M. Johnson, D. Herold, D. Farmer, and R. Pawlowicz. Real-time frontal mapping with AUVs in a coastal environment. In *IEEE Oceans*, pages 1094–1098, 1996.
- [26] Rutgers University Marine Field Station. <http://www.marine.rutgers.edu>, 1998.
- [27] L. Sternick. Velocity determination by Doppler sonar in deep water. *IEEE Trans. Aerospace and Electronic Systems*, pages 265–271, November 1978.
- [28] R. Stokey and T. Austin. Sequentail, long baseline navigation for REMUS, an autonomous underwater vehicle. In *SPIE International Symposium on Information systems for Navy divers and autonomous underwater vehicles operating in the surf zone*, volume 3711, pages 3711–25, 1999.
- [29] C. Tyren. Magnetic anomalies as a reference for ground-speed and map-matching navigation. *The Journal of Navigation*, 35(2):242–254, May 1982.
- [30] J. Vaganay, J. G. Bellingham, and J. J. Leonard. Outlier rejection for autonomous acoustic navigation. In *Proc. IEEE Int. Conf. Robotics and Automation*, pages 2174–2181, April 1996.

- [31] J. Vaganay, J. G. Bellingham, and J. J. Leonard. Comparison of fix computation and filtering for autonomous acoustic navigation. *International Journal of Systems Science*, 29(10):1111–1122, October 1998.
- [32] C. von Alt, B. Allen, T. Austin, and R. Stokey. Remote environmental monitoring units. In *AUV 94*, 1994.
- [33] L. Whitcomb, D. Yoerger, and H. Singh. Advances in Doppler-based navigation of underwater robotic vehicles. In *IEEE J. Robotics and Automation*, pages 399–406, Detroit, MI, May 1999.
- [34] D. Yoerger, A. Bradley, and B. Walden. High resolution mapping of a fast spreading mid ocean ridge with the autonomous benthic explorer, abe. In *Proc. Int. Symp. on Unmanned Untethered Submersible Technology*, pages 21–31, 1999.